

PrivacyProber: Assessment and Detection of Soft–Biometric Privacy–Enhancing Techniques

Peter Rot, *Member, IEEE*, Peter Peer, *Senior Member, IEEE*, and Vitomir Štruc, *Senior Member, IEEE*

Abstract—Soft–biometric privacy–enhancing techniques represent machine learning methods that aim to: (i) mitigate privacy concerns associated with face recognition technology by suppressing selected soft–biometric attributes in facial images (e.g., gender, age, ethnicity) and (ii) make unsolicited extraction of sensitive personal information infeasible. Because such techniques are increasingly used in real–world applications, it is imperative to understand to what extent the privacy enhancement can be inverted and how much attribute information can be recovered from privacy–enhanced images. While these aspects are critical, they have not been investigated in the literature. We, therefore, *study the robustness* of several state–of–the–art soft–biometric privacy–enhancing techniques to attribute recovery attempts. We propose PrivacyProber, a high–level framework for restoring soft–biometric information from privacy–enhanced facial images, and apply it for attribute recovery in comprehensive experiments on three public face datasets, i.e., LFW, MUCT and Adience. Our experiments show that the proposed framework is able to restore a considerable amount of suppressed information, regardless of the privacy–enhancing technique used, but also that there are significant differences between the considered privacy models. These results point to the need for novel mechanisms that can improve the robustness of existing privacy–enhancing techniques and secure them against potential adversaries trying to restore suppressed information.

Index Terms—face recognition, privacy, deep learning, computer vision, robustness analysis

1 INTRODUCTION

FACIAL images represent a rich source of information, from which a multitude of attributes can be extracted automatically using contemporary machine learning models, including gender, age, ethnicity, affective state, or even body mass indices [1], [2], [3], [4], [5], [6], [7], [8]. However, with the rapid proliferation of automatic recognition techniques in facial analytics, privacy–related concerns have also emerged and now represent a *key challenge with regards to the trustworthiness* of the technology [9], [10].

To address these concerns, researchers are increasingly looking into *privacy–enhancing* mechanisms capable of ensuring a trade–off between the utility of the data for facial analytics, on the one hand, and privacy protection, on the other [11], [12], [13], [14], [15], [16]. Of particular interest here are so-called *soft–biometric privacy–enhancing techniques*, which aim to perturb (transform, modify) facial images in a way that makes it difficult (or impossible) for automatic machine learning techniques to infer sensitive attributes (e.g., gender, age, ethnicity), while making only minimal changes to the visual appearance of the images. As a result, the privacy–enhanced (perturbed, tampered) images can be shared online (e.g., on social media), but do not allow for automatic user profiling, attribute extraction and other

unsolicited forms of processing. Such privacy–enhancing mechanisms represent pivotal tools for addressing societal expectations about the appropriate use of personal data, but also for meeting safeguards and standards defined in data–protection legislation and privacy acts, such as, GDPR [17], CCPA [18], BIPA [19] and others [13].

Several powerful techniques have been proposed in the literature for ensuring soft–biometric privacy and preventing automatic extraction of facial attributes, including synthesis–based techniques [20], auto–encoder based models [11], [21] or adversarial perturbations [12], [22]. While these techniques have been shown to successfully obscure soft–biometric information for selected attribute classifiers, experimental performance evaluations are typically limited to vanilla (or zero–effort) evaluation scenarios, where no attempt is made to reconstruct the obscured attributes. Due to this practice, it is not clear if the privacy levels reported in the literature generalize to real–world applications, where a potential adversary may exploit additional knowledge and invest considerable effort and resources to recover the concealed information. Such zero–effort evaluations, hence, *raise questions about the reliability* of existing privacy models¹ and their sensitivity to attribute recovery attempts. Comprehensive reliability studies are, therefore, critical for better understanding the capabilities of contemporary privacy–enhancing techniques and have implications for their deployment in practice. However, to the best of our knowledge, such studies are largely missing from the literature.

In this paper, we try to address this gap and explore possibilities for recovering obscured (concealed, suppressed) information from privacy–enhanced facial images with the

- P. Rot is with the Faculty of Electrical Engineering as well as with the Faculty of Computer and information Science, University of Ljubljana, Ljubljana, Slovenia, Corresponding author e-mail: peter.rot@fe.uni-lj.si
- P. Peer is with the Faculty of Computer and information Science, University of Ljubljana, Večna Pot 113, 1000 Ljubljana, Slovenia.
- V. Štruc is with the Faculty of Electrical Engineering, University of Ljubljana, Tržaška cesta 25, 1000 Ljubljana, Slovenia.

1. The term privacy model is used as a synonym for biometric privacy–enhancing technique in this paper for brevity.

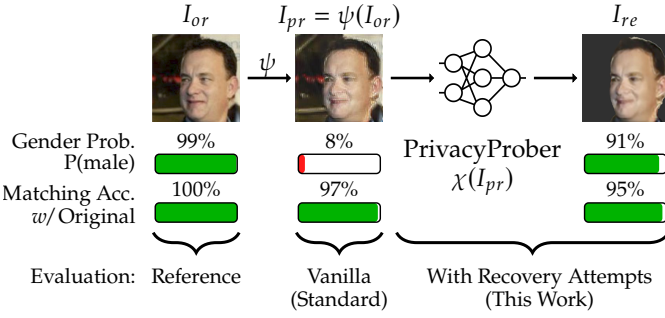


Fig. 1: The performance of soft-biometric privacy models, ψ , is commonly evaluated by comparing attribute classification performance over the original (reference) face images, I_{or} , and their privacy-enhanced counterparts, I_{pr} . In this paper we study the robustness of existing privacy models beyond such vanilla evaluation scenarios and propose an attribute recovery framework, called PrivacyProber, that allows for more comprehensive evaluations using images with reconstructed soft-biometric information, I_{re} . The bottom part of the figure visualizes the idea through illustrative gender predictions (i.e., probabilities of being male) and the match scores between I_{or} and the transformed images, I_{pr} and I_{re} . Note the difference in gender predictions for the different tasks with and without attribute recovery.

goal of assessing the reliability and robustness of existing soft-biometric privacy models. To facilitate the study, we develop an attribute recovery framework, called *PrivacyProber*, which uses various types of image transformations (learned over clean, non-tampered images) to reconstruct suppressed information from privacy-enhanced facial images. The proposed framework is based on minimal (black box) assumptions and requires no examples of privacy-enhanced images to restore soft-biometric information, which makes it applicable to a wide variety (of conceptually different) privacy models. To demonstrate the feasibility of our framework, we conduct extensive experiments with multiple state-of-the-art privacy models and three publicly available face datasets. Our experimental results show that PrivacyProber is able to recover a considerable amount of suppressed attribute information and that sensitivity to reconstruction attacks is still a considerable issue with existing privacy-enhancing techniques. As an additional contribution, we also show that the proposed framework can be used to *detect privacy-enhancement* in facial images, pointing to another threat vector with respect to existing privacy models that allows for flagging tampered images and treating them differently from non-tampered data, e.g., using manual screening.

As part of our reliability study (illustrated in Fig. 1), we make the following main contributions:

- We conduct, to the best of our knowledge, the *first comprehensive investigation* into the robustness of soft-biometric privacy-enhancing techniques with respect to attribute recovery attempts. We show that despite recent progress in this area, a considerable amount of concealed information can be recovered from (most) privacy-enhanced images, but also that there are significant differences in terms of robustness between the

tested privacy models.

- We propose *PrivacyProber*, a high-level framework for attribute recovery from privacy-enhanced facial images. The framework relies on dedicated reconstruction schemes build around inpainting, super-resolution, denoising, and face parsing models and requires no access to the evaluated privacy-enhancing techniques or prior knowledge about their inner workings.
- We present *novel methodology* to evaluate the robustness of soft-biometric privacy models. Specifically, we introduce an *attribute-recovery robustness (ARR)* score that reflects the robustness of privacy-enhancing techniques by comparing attribute-classification accuracy over reference and attribute-recovered images. We demonstrate the value of ARR scores through extensive experimentation with multiple privacy models and datasets.
- We show that PrivacyProber can be used to detect privacy-enhancement in facial images and propose an original detection approach, called *Privacy-enhancement Detection with Prediction Divergence (PD²)*, that relies on the Kullback-Leibler divergence between the probability predictions of an attribute classifier applied to facial images before and after attribute recovery. We show that PD² makes it possible to detect privacy-enhanced images with high accuracy and that it generalizes well across different data characteristics and privacy models.

2 BACKGROUND AND RELATED WORK

In this section we provide background information on the topic of soft-biometric privacy enhancement and review relevant prior work. For a more comprehensive coverage of the broader field of visual privacy and privacy protection of facial images the reader is referred to some of the excellent recent surveys in this area, e.g., [13], [23], [24], [25], [26].

2.1 Problem Definition and Model Taxonomy

Soft-biometric privacy-enhancement can formally be described as follows: given an original face image, $I_{or} \in \mathbb{R}^{w \times h}$, with w and h denoting the width and height of the image in pixels, and an arbitrary attribute classifier $\xi_a : \mathbb{R}^{w \times h} \mapsto \{a_1, a_2, \dots, a_N\}$, with the attribute labels $\{a_i\}_{i=1}^N$ corresponding to classes $\{C_1, C_2, \dots, C_N\}$, the goal of soft-biometric privacy-enhancement, ψ , is to generate privacy-enhanced images, $I_{pr} = \psi(I_{or})$, from which ξ_a cannot correctly predict the class labels a_i . Because ψ aims to obscure attribute information from automatic classification techniques without significantly affecting the perceptual quality of the images for human observers, an additional constraint is commonly considered in the design of ψ , i.e., that the perturbed images are as close as possible to the originals, $I_{pr} \approx I_{or}$. These characteristics are also illustrated on the left part of Fig. 1.

From a conceptual point of view, existing soft-biometric privacy-enhancing techniques can be categorized into two distinct groups: (i) techniques that try to induce incorrect attribute predictions, and (ii) techniques that try to generate approximately equal class probabilities for all attributes. Solutions from the first group typically rely on adversarial perturbations (and related strategies) and enhance privacy

by inducing misclassifications, i.e., $\xi_a(I_{pr}) \neq \xi_a(I_{or})$, where an incorrect attribute class label is predicted from I_{pr} with high probability. Techniques from the second group, on the other hand, commonly rely on (input-conditioned) synthesis methods that enhance privacy by altering image characteristics in a way that makes attribute predictions unreliable, i.e., $p(C_1|I_{pr}) \approx p(C_1|I_{pr}) \approx \dots \approx p(C_N|I_{pr})$, where $p(C_i|I_{pr})$ represents the posteriors of the attribute classes given the privacy-enhanced image I_{pr} generated by ξ_a . We review recent techniques from both groups below.

2.2 Soft-biometric Privacy Models

A considerable amount of research has been presented in the literature recently that addresses different problems related to soft-biometric privacy [11], [14], [16], [22], [27], [28], [29], [30]. Mirjalili and Ross [31], for example, developed a privacy-enhancing technique that perturbs gender information in facial images. The technique first performs Delaunay triangulation (over facial landmarks) to represent faces in the form of triangles that can be manipulated with goal of protecting privacy. Next, the texture within the triangles is optimized, such that a targeted gender classifier produces unreliable classification results, while the input image is only perturbed slightly. The authors showed that such an approach leads to image perturbations that can efficiently suppress gender information but have only a minimal effect on verification accuracy.

Another notable technique for soft-biometric gender privacy was presented in [21]. Here, the authors proposed Semi-Adversarial Networks (SANs) that rely on *conditional image synthesis* to obscure gender information. SANs represent convolutional auto-encoders paired with two discriminators that steer the synthesis process – one for enforcing gender privacy and the second for retaining verification accuracy (i.e., image similarities). The reported results suggest that the proposed SAN models are able to efficiently suppress gender information in facial images, while retaining high-levels of data utility for verification purposes. An extension to this work, called FlowSAN [11], was also presented later by the same authors to improve the generalization capabilities of SANs to unseen classifiers. The main idea of this work was to utilize multiple SAN transformations successively with the goal of making the privacy enhancement less dependent on a single target (gender) classifier. FlowSAN models were shown to offer better generalization capabilities than the simpler one-stage SANs, while still offering a highly competitive trade-off between privacy enhancement and utility preservation.

To make SAN models applicable beyond the (binary) problem of gender privacy that was at the core of most previous research on soft-biometric privacy, Marialli *et al.* [14] introduced PrivacyNet [14], an advanced SAN model build around Generative Adversarial Networks (GANs). Unlike competing solutions, PrivacyNet was shown to be capable of soft-biometric privacy enhancement with respect to multiple facial attributes, including race, age and gender. The model, hence, generalized the concept of SAN-based privacy enhancement to arbitrary combinations of soft-biometric attributes. We note at this point that the SAN-based family of algorithms is not based on adversarial per-

turbations, but relies on *facial synthesis* facilitated by auto-encoders driven by a number of competing discriminators.

An approach for privacy enhancement of k facial attributes via adversarial perturbations (k -AAP) was described by Chhabra *et al.* in [12]. The proposed approach tries to infuse facial image with so-called adversarial noise with the goal of suppressing a predefined set of arbitrary selected facial attributes, while preserving others. k -AAP is based on the Carlini Wagner L2 attack [32] and achieves promising results with attribute classifiers that were included in the construction of the adversarial noise. The approach results in image perturbations (for most images) that are efficient at obscuring attribute information for machine learning models, but are imperceptible to the human eye. However, similarly as the original version of SAN, k -AAP does not generalize well to arbitrary classifiers. The idea of flipping facial attributes using adversarial noise was also explored in [22] where the authors investigated the robustness of facial features perturbations generated by the Fast Gradient Sign Method (FGSM) method [33].

2.3 Evaluation of Soft-biometric Privacy Models

Quantifying the level of privacy enhancement is a challenging task and requires well-defined evaluation methodologies and corresponding performance scores that provide insight into the characteristics of the tested privacy models. To quantify performance, most of the existing work in this area relies on automatic recognition techniques trained for extracting various facial attributes. Recognition experiments are then conducted on the original and privacy-enhanced data and differences in the observed classification accuracies are used for performance reporting [11], [14], [16], [29], [30].

Additionally, several scalar performance scores have also been proposed in the literature. Othman and Ross [20], for example, introduced *gender suppression levels*, a performance score for measuring the success of a synthesis-based privacy-enhancing technique with respect to the induced misclassification of gender. Dhar *et al.* [34] studied how state-of-the-art recognition models process soft-biometric information and explored how much sensitive information is encoded in different layers of a deep face recognition model. They proposed *expressivity* as a measure of how much information a given representation carries about a selected face attribute. Terh rst *et al.* proposed the *privacy-gain identity-loss* coefficient (PIC), which measures the gain of privacy with respect to a chosen facial attribute (e.g. gender) but takes the retained verification utility into the account as well. The same authors also proposed [30] *correct overall/female/male classification rates* (COCR/CFCR/CMCR) to score the success of privacy-enhancing algorithms. More recently, the authors of [28] proposed a set of evaluation protocols with associated performance measures to enable reproducible research on soft-biometric privacy.

While the evaluation methodologies reviewed above provide initial estimates about the performance of biometric privacy-enhancing techniques, they only assume zero-effort evaluation scenarios. In this study, we built on the presented work and propose a more comprehensive evaluation methodology that also considers attribute reconstruction attempts when scoring privacy models. We introduce a

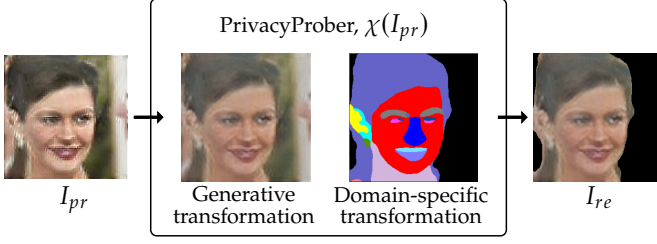


Fig. 2: High-level illustration of PrivacyProber. Generative and domain-specific transformations are used (separately or in sequence) to recover attribute information concealed/suppressed by soft-biometric privacy models.

novel performance measure that captures the robustness of the models and offers insight into the difficulty of recovering concealed attribute information.

2.4 Detection of Privacy Enhancement

Soft-biometric privacy enhancing techniques introduce changes to the visual characteristics of facial images and can, hence, be seen as a form of image tampering. While a considerable body of work has been presented in the literature to detect such tampering, e.g. [35], [36], [37], such detection techniques have been mostly considered by the digital forensics community. The problem of detecting privacy enhancement, on the other hand, is new and has not been addressed before in the open literature. Because some privacy models are based on adversarial perturbations, this problem is also partially related to adversarial attack detection methods [38], [39], [40], [41], [42]. However, because soft-biometric privacy enhancement also includes synthesis-based methods (among others), as discussed in Section 2.2, the problem of detecting such image modifications is considerably broader.

3 PRIVACYPROBER

In this section, we describe the proposed PrivacyProber, a framework for the recovery of suppressed soft-biometric attribute information from privacy enhanced face images.

3.1 Overview of PrivacyProber

Existing evaluation schemes for soft-biometric privacy models typically compare the performance of an attribute² classifier $\xi_a(\cdot)$, when applied to the original $\xi_a(I_{or})$ and privacy enhanced images $\xi_a(I_{pr})$. While the observed performance difference provides a first estimate of the level of privacy ensured by the privacy models, it also assumes that no attempt is made to recover the information initially contained in the input image I_{or} . As a result, the privacy levels empirically determined with such vanilla evaluation methodology may be overestimated and not representative of the actual capabilities of existing privacy models.

2. Common attributes considered in the literature include *gender*, *age*, or *ethnicity*.

The proposed PrivacyProber, described below, tries to address this problem by facilitating performance assessments beyond zero-effort evaluation experiments. Specifically, PrivacyProber seeks to recover concealed image information by transforming privacy-enhanced images I_{pr} in such a way that the privacy enhancement is reversed, or formally, such that the classifier $\xi_a(\cdot)$ generates the same predictions for the original, I_{or} , and recovered images, I_{re} , i.e.:

$$\xi_a(I_{or}) = \xi_a(\chi(I_{pr})), \quad (1)$$

where $I_{re} = \chi(I_{pr})$ and $\chi(\cdot)$ is the transformation applied by the PrivacyProber. By estimating the level of privacy through performance differences of the attribute classifier $\xi(\cdot)$ applied to the original $\xi(I_{or})$ and attribute-recovered images $\xi_a(I_{re})$, where $I_{re} = \chi(I_{pr})$, a more informative estimate of privacy-enhancement performance (or robustness) can be obtained. The main idea is presented in Fig. 1.

While in general, the transformation $\chi(\cdot)$ could be learnt in a data-driven manner by defining a loss penalizing the difference in classification outputs between $\xi(I_{or})$ and $\xi(\chi(I_{pr}))$, such an approach is (i) model-specific and not universally applicable, (ii) requires access to training data for each considered privacy model, and (iii) warrants prior knowledge about the internal mechanism governing the privacy-enhancement procedure. In this paper we, therefore, follow a more general approach and design PrivacyProber under the following (minimal) assumptions:

- **Black-box privacy models:** We assume no information about (or access to) the privacy models is available. We only exploit the fact that the privacy models aim to suppress soft-biometrics information, while making minimal changes to the appearance of the images.
- **Target domain:** We assume that privacy-enhancement is applied within a fixed image domain, i.e., on facial images, and not on images of arbitrary scenes.

Thus, we construct PrivacyProber based on a set of (i) *generative* and (ii) *domain-specific* transformations, which can be used separately or in sequence, as illustrated in Fig. 2. In the next sections we propose several possibilities for recovering suppressed soft-biometric attributes from privacy-enhanced images using such transformations.

3.2 Generative transformations

Soft-biometric privacy-enhancing techniques modify or partially corrupt the visual content in the original images I_{or} with the goal of reducing the utility of the data for some targeted attribute classification task. The use of generative transformations³ for mitigating such image tampering is motivated by the fact that prior information about (clean, non-tampered) original face images can be incorporated efficiently into generative models (without the need for examples of privacy-enhanced images) and exploited for attribute recovery. Similar approaches have also proven useful for protection against adversarial attacks [43], [43], [44]. We propose three generative transformations for implementing PrivacyProber based on (i) *inpainting*, (ii) *denoising*, and (iii) *super-resolution*.

3. Note that we use the term *generative transformation* loosely here to account for the transformation considered in this group, which include inpainting, super-resolution and denoising.

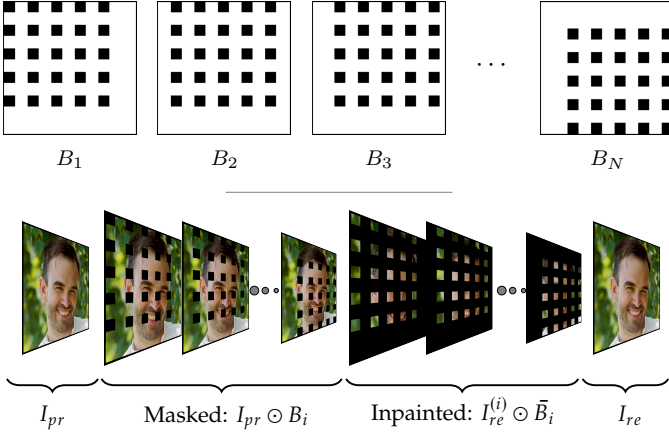


Fig. 3: Illustration of the inpainting-based attribute recovery procedure, χ_{in} , proposed for PrivacyProber. The privacy-enhanced image, I_{pr} , is masked N times with the binary masks B_i – shown in the top row. The masked regions are then inpainted based on the remaining context. Finally, the attribute-recovered image I_{re} is reconstructed from the inpainted regions only.

3.2.1 Attribute Recovery Through Inpainting

Inpainting models typically aim to fill in missing pixels in a damaged image and to restore the corrupted content. Our goal, on the other hand, is to recover a complete image I_{re} from I_{pr} with attribute information restored and not just a small portion of the data. We, therefore, design a dedicated inpainting strategy for this task that sequentially inpaints small parts of the image at the time and then aggregates the results to recover the complete image. The basic assumption with this attribute-recovery strategy is that inpainting can restore (clean) non-tampered content by inferring pixels from contextual information even if this information was tampered with by a soft-biometric privacy-enhancing model.

The proposed recovery procedure, illustrated in Fig. 3, starts with the privacy-enhanced image $I_{pr} \in \mathbb{R}^{w \times h}$ and a set of N binary masks $B_i \in \mathbb{R}^{w \times h}$, where w and h again denote the width and height of the image, respectively, and $i \in \{1, 2, \dots, N\}$. The binary masks are initialized as matrices of all ones. Next, a chess-like pattern composed of multiple square regions (of size $d \times d$, where $d \ll \{w, h\}$) is constructed and placed into the initialized masks. Pixels in B_i corresponding to the chess-like pattern are set to zero. As illustrated in the top row of Fig 3, the pattern is positioned in the top right corner for the first mask and then shifted N -times in a sliding-window manner (with overlap), such that all positions are traversed in both the horizontal and vertical direction. To facilitate inpainting, the constructed binary masks B_i are then used to remove pixels from the privacy-enhanced image, i.e.:

$$I_{pr}^{(i)} = I_{pr} \odot B_i, \text{ for } i \in \{1, 2, \dots, N\}, \quad (2)$$

where \odot represents the Hadamard product and $I_{pr}^{(i)}$ denotes the input image masked by B_i . In the next step, all pixels set to zero are reconstructed using a predefined inpainting model, which given a set of masked images $\{I_{pr}^{(i)}\}_{i=1}^N$ generates a set of corresponding (partially) recovered images

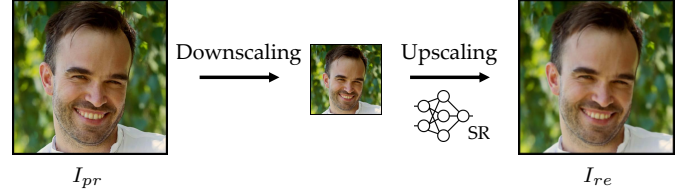


Fig. 4: Illustration of the super-resolution based attribute recovery procedure, χ_{sr} , proposed for PrivacyProber. The privacy-enhanced image, I_{pr} (on the left), is first downsampled to a smaller scale with the goal of removing high-frequency components. High-frequency information is then infused back into the recovered image, I_{re} (on the right), in a selective manner through a super-resolution model.

$\{I_{re}^{(i)}\}_{i=1}^N$. Finally, the complete attribute-recovered image I_{re} is reconstructed from the inpainted regions only:

$$I_{re} = [I_{re}^{(i)} \odot \bar{B}_i]_{i=1}^N, \quad (3)$$

where \bar{B}_i is an inverted version of B_i used to exclude the original (non-inpainted) areas from $I_{re}^{(i)}$ and $[\cdot]$ represents an averaging operation over non-zero pixels. This type of averaging is needed due to the overlap in the masked regions between binary masks. We denote the presented attribute-recovery procedure as $\chi_{in} : I_{pr} \mapsto I_{re}$ hereafter and implement it using an off-the-shelf inpainting model.

3.2.2 Attribute Recovery Through Denoising

The second proposed approach to attribute recovery is based on denoising. Soft-biometric privacy-enhancing techniques typically aim to make only minute changes to the input images, I_{or} , and alter their visual characteristics as little as possible. The changes introduced can, therefore, be well accounted for by the high-frequency part of the privacy-enhanced images I_{pr} . We model these high-frequency alterations as noise and try to remove them using a denoising procedure. Such denoising strategies have proven useful for removal of adversarial noise [43], and are, therefore, also expected to be useful for reversing soft-biometric privacy enhancement that shares characteristics with techniques based on adversarial examples. Similarly as in the previous section, we denote the denoising-based attribute-recovery procedure as $\chi_d : I_{pr} \mapsto I_{re}$ hereafter and again implement it using an off-the-shelf inpainting model.

3.2.3 Attribute Recovery Through Super-Resolution

The last generative approach to attribute recovery proposed in this work is based on super-resolution (or better said face hallucination⁴). Super-resolution can be seen as a restoration approach that selectively adds specific details (high-frequency components) to low-resolution input images. Because these high-frequency details are added in a selective manner based on learnt correspondences between pairs of low- and high-resolution facial images, images subjected to super-resolution are in essence remapped to a higher resolution, which impacts image characteristics, including those infused by privacy enhancement.

4. Single image super-resolution methods applied to facial images are commonly referred to as face hallucination methods [45], [46].

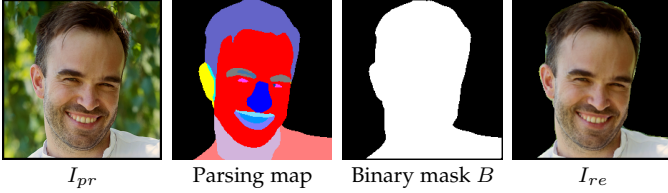


Fig. 5: Illustration of the domain-specific attribute recovery procedure, χ_{br} , proposed for PrivacyProber. The privacy-enhanced image, I_{pr} , is masked with a binary mask B that corresponds to the facial region. Because the background is partially affected by the privacy enhancement, focusing only on the facial area impacts the behavior of attribute classification models.

To exploit super-resolution for attribute recovery, we propose a straight-forward two-step procedure, as illustrated in Fig. 4. In the first step, the input image, $I_{pr} \in \mathbb{R}^{w \times h}$ is downsampled by a factor s , i.e.:

$$I_{pr}^{(s)} = f_s(I_{pr}), \quad (4)$$

where $f_s(\cdot)$ is a bilinear downsampling function conditioned on s and $I_{pr}^{(s)} \in \mathbb{R}^{w_s \times h_s}$ is the downsampled image with $w_s < w$ and $h_s < h$. This downsampling acts as a low-pass filter that removes high-frequency information from the image, similarly to the denoising procedure discussed above. The second step then restores the downsampled image to its original size and recovers semantically meaningful image details (with attribute information) through a super-resolution operation, i.e.:

$$I_{re} = h_s(I_{pr}^{(s)}), \quad (5)$$

where h_s represents a super-resolution model that upscales images by a factor of s . We denote the super-resolution-based attribute-recovery procedure as $\chi_{sr} : I_{pr} \mapsto I_{re}$ and use a state-of-the-art model for our implementation.

3.3 Domain-specific transformation

Instead of building on generative models trained on clean non-tampered data to restore facial attributes, another possibility is to base attribute recovery on specifics of the targeted image domain. With facial images, for example, automatic attribute inference should be based solely on the facial region and ignore other contextual information, e.g., background. With domain-specific transformations we, hence, aim to incorporate information on facial semantics into the attribute-recovery procedure and exclude image regions irrelevant for attribute classification from the data.

We propose one domain-specific transform in this work that relies on face parsing. Specifically, given an arbitrary face parser f_p , we extract facial-part information from the privacy-enhanced image I_{pr} and aggregate all part labels that corresponds to the facial region into a binary mask B . The labeled facial parts produced by the face parser and the corresponding binary mask are illustrated in Fig. 5. Once the binary mask is constructed, it is utilized to exclude background pixels from the image with the goal of making attribute inference less susceptible to artifacts generated by the privacy enhancement:

$$I_{re} = I_{pr} \odot B, \quad (6)$$

where \odot is gain the Hadamard product. This type of attribute recovery is denoted as $\chi_{br} : I_{pr} \mapsto I_{re}$ hereafter.

3.4 Beyond Zero-effort Evaluation Scenarios

PrivacyProber, χ , can in general be implemented using any combination of the transformations discussed above $\{\chi_{in}, \chi_d, \chi_{sr}, \chi_{br}\}$ and utilized to explore the robustness of a given soft-biometric privacy model to attribute recovery attempts. A general high-level framework for using the proposed PrivacyProber in evaluation scenarios that go beyond zero-effort recognition experiments is given under Algorithm 1.

Algorithm 1 Privacy evaluation with PrivacyProber

Input: Attribute classifier ξ_a , set of N input images $\{I_{or}\}_N$, privacy model ψ

Output: Performance (robustness) estimate for ψ

Implement PrivacyProber, χ , from $\{\chi_{in}, \chi_d, \chi_{sr}, \chi_{br}\}$

for Each image in $\{I_{or}\}_N$ **do**
 Apply privacy model: $I_{pr} = \psi(I_{or})$
 Attempt attribute recovery: $I_{re} = \chi(I_{pr})$
 Use ξ_a for classification over I_{or} and I_{re} ;
end

Calculate performance of ξ_a over $\{I_{or}\}_N$ and $\{I_{re}\}_N$

Estimate robustness of ψ based on results (see Section 4.2 for scoring methodology)

4 EVALUATION OF PRIVACY MODELS

In this section we evaluate several state-of-the-art privacy enhancing techniques using standard vanilla methodology as well as the proposed PrivacyProber. The goal of these experiments is to provide insight into the performance, but more importantly robustness of biometric privacy models and to demonstrate the importance of experimental evaluations that go beyond zero-effort recognition experiments. Furthermore, we also demonstrate how the proposed PrivacyProber can be used to detect privacy enhancement (tampering) in facial images – something that (to the best of our knowledge) has not yet been attempted in the literature.

4.1 Considered Privacy Models

Three recent (soft-biometric) privacy-enhancing techniques are implemented for the experiments, i.e., the k -AAP method from [12], the FGSM-based technique from [47] and the FlowSAN approach from [11]. Because FlowSAN can strike a balance between the level of privacy protection ensured and the preserved utility of the facial images, two different versions of the model are considered: *i*) one with three SAN models arranged sequentially one after the other (FlowSAN-3 hereafter), and *ii*) one with five sequential SAN models (FlowSAN-5). All four techniques are trained to obscure *gender information*, which is also the most frequently considered attribute in research addressing soft-biometric privacy [11], [16], [20], [30]. The techniques are selected for the experiments because of their state-of-the-art performance and the fact that they rely on different mechanisms for ensuring soft-biometric privacy. As such, they serve as

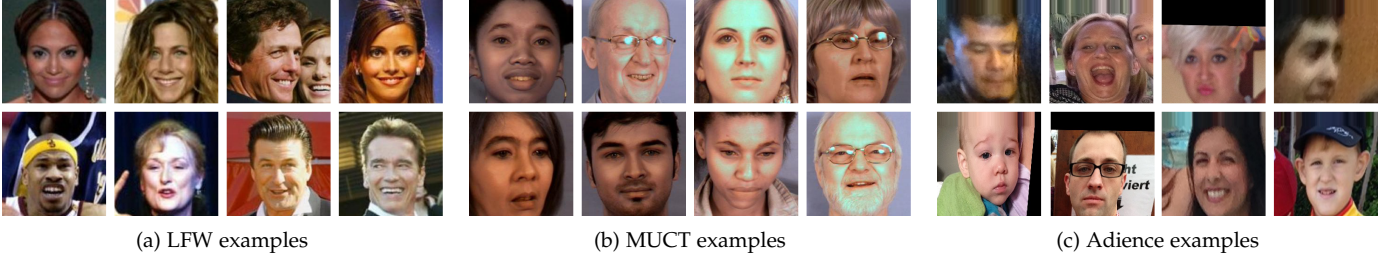


Fig. 6: Sample face images from the datasets used in the experiments. The selected datasets contain faces with different demographic characteristics that are usually targeted by soft-biometric privacy enhancing techniques. As can be seen, the datasets were captured in challenging and diverse (real-world) imaging conditions.

a representative cross-section of exiting techniques and contribute towards demonstrating the importance of evaluating biometric privacy models beyond zero-effort recognition experiments.

4.2 Datasets, Setup, and Performance Measures

To assess the performance of the considered privacy models, three publicly available face datasets are used, i.e., Labeled Faces in the Wild (LFW) [48], MUCT [49], and Adience [50]. The datasets ship with the needed gender labels and contain challenging facial images captured in a wide variety of imaging conditions, as illustrated in Fig. 6. Moreover, they represent standard datasets for assessing the performance of existing privacy-enhancing techniques (e.g., [11], [14], [15], [16]) and are, therefore, also used in this work.

All images are roughly aligned prior to the experiments such that the faces are cropped to exclude background pixels and then rescaled to a standard size of 224×224 pixels. The preprocessed images are subjected to privacy enhancement and used in the experimental assessment to evaluate the following aspects of the privacy models:

- (a) **Level of soft-biometric privacy enhancement:** The performance of the evaluated privacy models is measured through gender (g) classification experiments with predefined classifiers on the original (o) and privacy-enhanced (p) images. The level of privacy enhancement achieved is determined by comparing ROC curves generated from the two image sets. Additionally, the *gender suppression rate* (SR) [27] is also reported and defined in this work as:

$$SR = \max \left(\frac{AUC_{go} - f(AUC_{gp})}{AUC_{go}}, 0 \right) \in [0, 1], \quad (7)$$

where AUC_{go} and AUC_{gp} denote the area under the ROC curve before and after privacy enhancement, respectively, and the normalization function $f(\cdot)$ corresponds to:

$$f(x) = \begin{cases} x - 0.5, & \text{if } x \geq 0.5 \\ x, & \text{otherwise} \end{cases}. \quad (8)$$

The above definition allows us to report performance for (gender) privacy models that aim to induce misclassifications (i.e., invert classifier predictions for binary problems – invert ROC curves) as well as for models trying to induce random gender-classification probabilities (i.e., targeting a random AUC score of

0.5) using a *single* performance measure. A SR value of 1 indicates perfect attribute (gender) suppression, whereas a value of 0 implies that the suppression has no effect. Evaluating privacy models with SR scores and the approach presented above corresponds to zero-effort (vanilla) evaluation strategies commonly seen in the literature [11], [21].

- (b) **Utility preservation:** Soft-biometric privacy-enhancing techniques aim to retain as much of the original image information as possible, while altering the visual appearance of the input images only slightly. In accordance with standard evaluation methodology [11], [14], [20], [30] utility preservation is, therefore, assessed through verification experiments on the original and privacy-enhanced images, where minimal differences in performance are expected. Because there exists a trade-off between utility preservation and attribute suppression, a quantitative measure taking both tasks into account is reported for the experiments. Specifically, a modified version of the *privacy-gain identity-loss coefficient* (PIC) is used in this work [16], [27], [28], i.e.:

$$PIC = SR - IL, \quad (9)$$

where the *identity loss* IL is defined with the degradation in verification performance after the privacy enhancement:

$$IL = \max \left(\frac{AUC_{vo} - AUC_{vp}}{AUC_{vo}}, 0 \right). \quad (10)$$

In the above equations AUC_{vo} and AUC_{vp} are the AUC scores of the verification experiments (v) generated with the original (o) and privacy-enhanced (p) images. PIC is bounded to $[-1, 1]$, with a PIC score of 1 implying an ideal trade-off, i.e., no loss in verification performance and perfect attribute suppression.

- (c) **Robustness:** While attribute suppression and utility preservation are standard aspects of privacy models typically evaluated in zero-effort evaluation scenarios, robustness of the models to attribute recovery attempts has so far seen limited attention in the literature. Here, we use the proposed PrivacyProber to recover information suppressed by the studied privacy models. Identity verification and gender classification experiments are then conducted after attribute recovery (r) and the generated ROC curves are analyzed to assess robustness. A scalar robustness measure is derived from the ROC

TABLE 1: Overview of the main dataset characteristics and image splits used in the experiments. To ensure balanced experimental data and avoid bias in the generated results, the image splits are (approximately) gender balanced. Subjects between the training and testing part are disjoint. Testing is performed over four disjoint data splits to be able to report confidence scores on the reported results .

Dataset	Totals				Training		Testing [†]			
	#Images	#Subj.	#AvgIm/Subj.	#Images (Gender)	#Images	#Subj.	#Images	#Subj.	#Mated	#Non-mated
LFW [48]	5,735	1,773	3.39	2,884 (m), 2,851 (f)	3,992	1,425	1,743	348	4,060	9,669,923
Adience [50]	10,502	1,395	9.22	5,238 (m), 5,264 (f)	8,493	1,006	2,009	389	4,029	9,640,738
MUCT [49]	3,693	522	13.38	1,803 (m), 1,890 (f)	3,119	276	574	246	1,191	1,027,277

[†] Totals over all 4 test data splits; #AvgIm/Subj – average number of images per subject; m – male, f – female;

curves in this paper, i.e., the *attribute–recovery robustness* (ARR), and reported in the experiments, i.e.:

$$ARR = g(AUC_{gp}) \cdot \frac{|AUC_{go} - AUC_{gr}|}{AUC_{go}} \quad (11)$$

where the subscripts suggest that the AUC score was computed from the recovered (*r*), privacy-enhanced (*p*) or original (*o*) images and $g(x)$, i.e.,

$$g(x) = \begin{cases} 2, & \text{if } x \geq 0.5 \\ 1, & \text{otherwise} \end{cases} \quad (12)$$

ensures that robustness is measured for all privacy models on the scale $[0, 1]$. Thus, ARR scores serve as a measure of robustness to attribute recovery attempts and take a value of 0 if after the recovery the same performance is achieved as with the original images and a value close to 1 if no information can be inferred from the privacy-enhanced images.

To facilitate the evaluation described above, the experimental datasets are split into training and testing parts. The training parts are used to train gender classifiers for each dataset and matchers for the verification experiments. Because the datasets are unbalanced with respect to gender, the number of male and female subjects in the training and testing sets is (approximately) balanced by randomly excluding images of the more represented gender. It is also made sure that at least two images per identity are present in the testing part for the verification experiments. To ensure a consistent evaluation setup across all datasets and be able to report confidence scores for the experiments, the test images are partitioned into 4 experimental splits. Gender recognition experiments are performed for every test image, while a fixed number of mated and non-mated comparison is performed for the verification experiments. Details on the experimental setup are provided in Table 1.

4.3 Baseline Evaluation of Privacy Models

The first series of experiments studies the performance of the considered privacy models using standard vanilla evaluation methodology. The goal of these experiments is to establish the baseline performance of the models and explore their characteristics.

4.3.1 Privacy vs. Utility

From an operational point of view, a critical aspect of (soft-biometric) privacy enhancement is the trade-off between privacy protection and utility preservation the models ensure. The first part of our evaluation, therefore, looks at this trade-off through a series of recognition experiments.

1) Baseline performance. To establish the baseline performance of the privacy models in terms of attribute suppression rates, a gender classifier ξ_g (a VGG16-based model with a two-class softmax at the top) is trained for each of the datasets and used to steer the privacy enhancement⁵. In accordance with standard evaluation methodology [12], [22], the same classifier is also used to evaluate gender recognition performance with the enhanced images on each dataset. Similarly, a ResNet-50 face recognition model [52] is learned for the utility preservation experiments on images from the VGGFace2 dataset. Here, the output of the last fully connected layer of the learned model is utilized as the feature representation of the input face images. The computed representations are then matched with the cosine similarity measure in verification experiments.

Fig. 7 shows ROC curves of the experiments on the three experimental datasets before and after privacy enhancement. Note that confidence intervals are not included to keep the plots uncluttered. Instead, standard errors are reported for the (scalar) performance scores in Fig. 8. As can be seen, the two privacy models that aim to induce misclassifications, *k*-AAP and FGSM, result in close to ideal gender suppression rates (SP) of 1 on all datasets, except for LFW, where the Carlini-Wagner attack used with *k*-AAP is not successful on several test images using our optimization parameters. The suppression rates for the FlowSAN models (which aim to produce random gender classification probabilities for each input image), on the other hand, depend on the number of SAN models used in the sequence. FlowSAN-3, for example, generates lower SR scores than FlowSAN-5, but is, therefore, retaining more identity information, as evidenced by the lower identity losses (ILs) in Fig 8. When comparing *k*-AAP and FGSM to the FlowSAN models, we observe that the former two models ensure higher overall PIC scores on most dataset (except LFW, where *k*-AAP is slightly below FlowSAN-5 in terms of PIC), but this is a consequence of the fact the the FlowSAN models do not simply invert classifier probabilities and, therefore, target a more challenging problem, which makes these models applicable to a wider range of application domains. Especially successful in terms of the privacy-utility trade-off is FGSM, which achieves PIC scores of close to 1 on all three datasets.

While most of the findings discussed above hold for all considered datasets, there are slight differences with the Adience dataset. Here, the verification as well as gender recognition performance with the original images is lower

5. For the FlowSAN models several such classifiers are trained using different training data configurations similarly to [51].

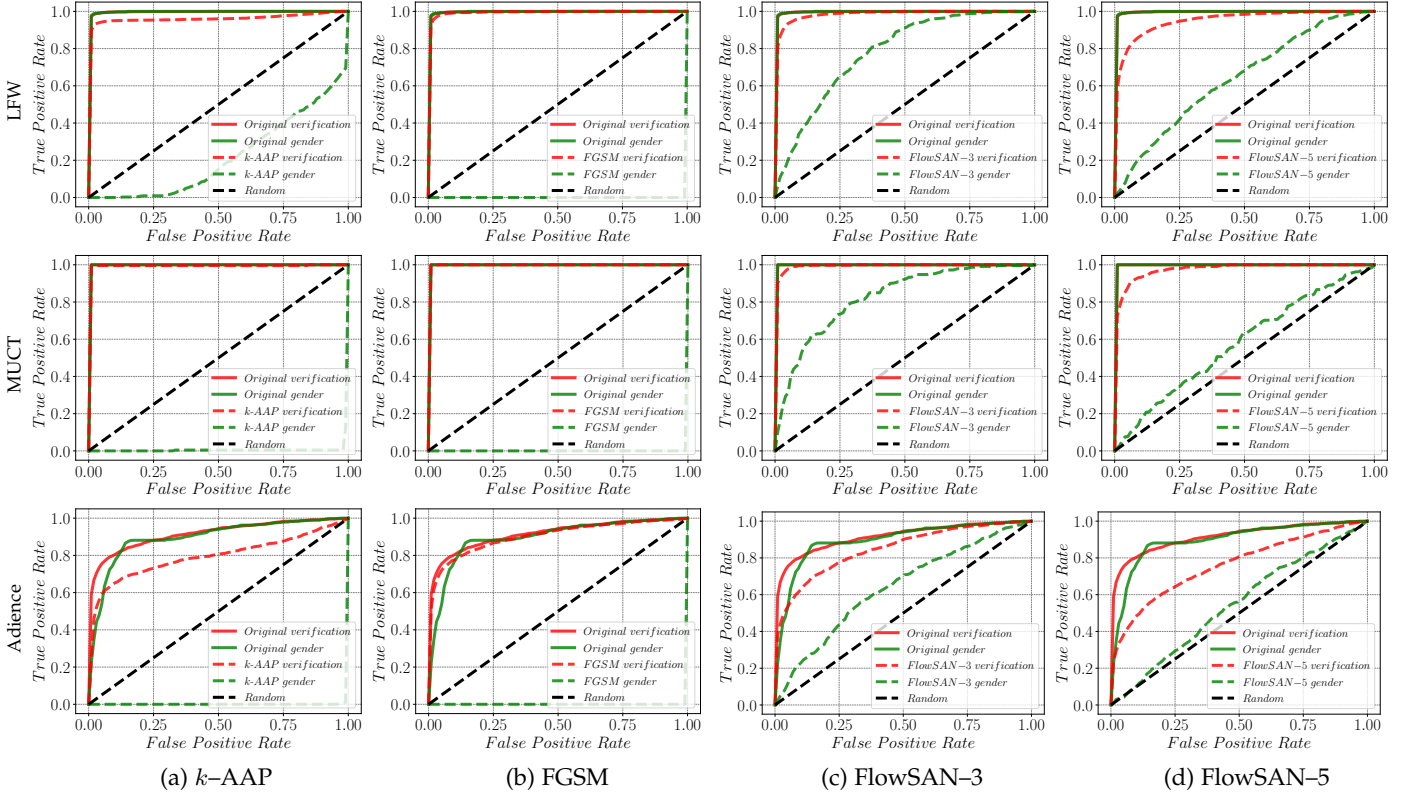


Fig. 7: ROC curves displaying the privacy vs. utility trade-off ensured by the evaluated privacy models. Results for different datasets are shown in rows and for different privacy models in columns. All evaluated models are in general able to retain a significant portion of the verification performance (red curves), while resulting in different gender suppression rates (green curves). Note again that k -AAP and FGSM aim to induce misclassifications (i.e., invert classifier predictions for binary problems), whereas the FlowSAN models aim to produce random gender classification results. The figure is best viewed in color.

compared to the other two datasets. This is due the characteristics of the dataset, which features real-world images with extreme appearance variations that differ significantly from those present in LFW and MUCT. As a result, even minor (additional) image degradations lead to significant performance drops, which is reflected in the relatively larger IL scores for all methods on this dataset.

2) Generalization to unseen classifiers. The result discussed above were generated with the same gender classifier, ξ_g , that was also used for privacy enhancement on each dataset. To evaluate the generalization ability of the privacy models to unseen classification models, a ResNet-50 gender classifier, ξ_g^u , is trained on LFW in the next series of experiments and deployed on the remaining two datasets, i.e., MUCT and Adience. Thus, the model used for scoring gender recognition accuracy differs in topology as well as training data from the model utilized for privacy enhancement.

Table 2 provides a summary of the PIC, SR and IL scores generated for this experiment. Here, the colored numbers show the relative change (marked as Δ) in the computed scores when compared to the baseline performance from Fig. 8. As expected, all privacy models degrade in performance, both in terms of PIC as well as SR score compared to the baseline experiments. The relative drop is quite severe for the adversarial techniques. The PIC scores drop by

17.8% on Adience and by 32.8% on MUCT for k -AAP, and by 23.4% on MUCT and 28.8% on Adience for FGSM. FlowSAN-3, on the other hand, achieves an increase of 3.3% in terms of PIC on MUCT and a drop of 5.3% on Adience. FlowSAN-5 results in larger performance degradations, but still less so than k -AAP or FGSM. Similar observations can also be made for the relative change in SR scores.

In terms of absolute values, the FlowSAN models achieve the highest gender suppression rates (SRs) on Adience with the tested classifier, and also outperform k -AAP and FGSM on MUCT. On Adience, which differs significantly in terms of data characteristics from LFW and MUCT, k -AAP is the top performer in terms of SR score. When considering the overall PIC score, FlowSAN-3 performs best among all tested methods on the Adience dataset, whereas FGSM performs best on the MUCT dataset. This result is largely a consequence of the fact that FGSM exhibits the lowest identity drop IL on Adience among all privacy models, leading to the most desirable privacy vs. utility trade-off on this dataset.

Overall, the results of these experiments suggest that all tested privacy models offer a certain level of robustness to unseen classifiers, but the relative drop in performance differs significantly from model to model. The FlowSAN models, which exploit several gender classifiers for (soft-biometric) privacy enhancement, appear to be more robust

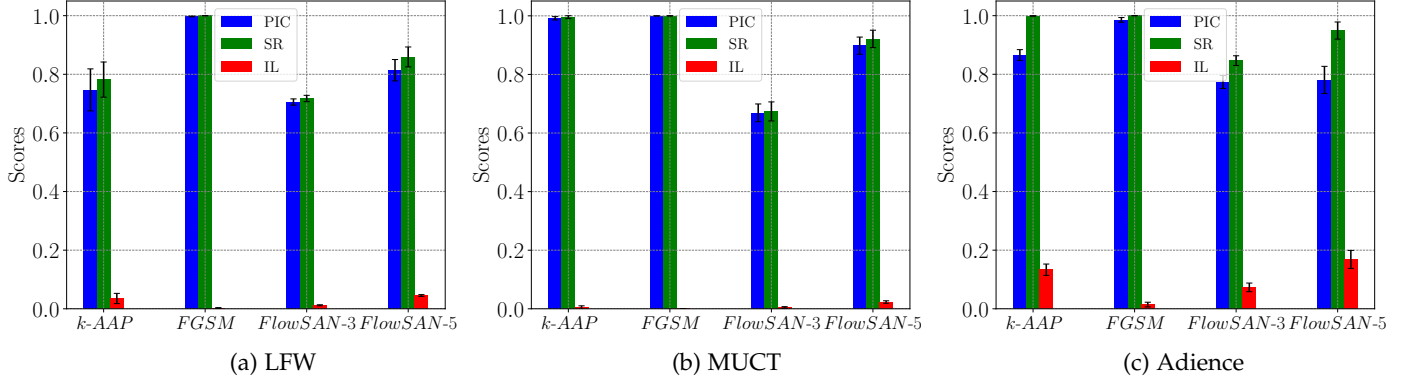


Fig. 8: Scalar performance indicators for the privacy vs. utility trade-off of the privacy models. Results are reported for three datasets and in the form of mean PIC (higher is better), SR (higher is better) and IL (lower is better) scores with corresponding standard errors computed over the 4 test splits - see Table 1 for the experimental setup.

TABLE 2: Generalization ability of the privacy models to an unseen gender classifier ξ_g^u . The reported results are computed with a gender classifiers that differs from the one used for privacy enhancement in terms of training data and model topology. Results are reported (in terms of $\mu \pm \sigma$ computed over 4 test data splits) for gender suppression (SR), identity loss (IL) and the the combined PIC score. The colored numbers show the relative change Δ of the mean score compared to the baseline performance, the arrows and colors indicate whether the score increased (up, blue) or decreased (down, red).

Privacy Model	Dataset	PIC	Δ PIC (in %)	SR	Δ SR (in %)	IL
k -AAP	MUCT	0.664 ± 0.028	32.8% ↓	0.668 ± 0.030	32.7% ↓	0.004 ± 0.006
	Adience	0.688 ± 0.039	17.8% ↓	0.822 ± 0.033	17.7% ↓	0.133 ± 0.019
FGSM	MUCT	0.766 ± 0.031	23.4% ↓	0.766 ± 0.031	23.4% ↓	0.000 ± 0.000
	Adience	0.698 ± 0.030	28.8% ↓	0.712 ± 0.032	20.6% ↓	0.014 ± 0.008
FlowSAN-3	MUCT	0.702 ± 0.071	3.3% ↑	0.707 ± 0.073	3.3% ↑	0.005 ± 0.003
	Adience	0.721 ± 0.281	5.3% ↓	0.794 ± 0.278	5.3% ↓	0.073 ± 0.015
FlowSAN-5	MUCT	0.709 ± 0.027	18.9% ↓	0.732 ± 0.025	18.9% ↓	0.023 ± 0.004
	Adience	0.643 ± 0.271	13.8% ↓	0.812 ± 0.265	13.7% ↓	0.169 ± 0.031

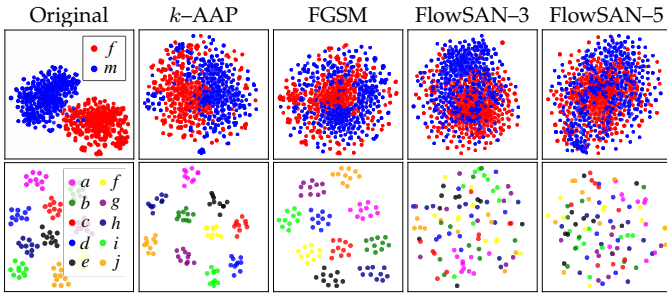


Fig. 9: t -SNE plots (in 2D) of gender and identity features. The gender plots in the top row are generated from 700 randomly sampled LFW images of each gender (f-female, m-male). The subject-conditioned distributions in the bottom row are generated based on 10 randomly selected images of the 10 largest classes from LFW (marked (a) – (j)). By comparing the distribution of the original and processed images the impact of the privacy enhancement can be observed.

to changes in the classification model used and may be preferred if no assumptions can be made regarding the target classifier used with the final application.

4.3.2 Feature Distribution Exploration

Next, we investigate the effect of privacy enhancement on the distribution of the features generated by the last fully connected layers of the (i) ResNet-50 face recognition model

and the (ii) VGG16 gender classifier. Here, the same setup is used as with the baseline experiments discussed above. The goal of this series of experiments is to better understand what is happening at the representation level as a result of the privacy enhancement and to gain additional insight into the characteristics of the privacy models. To study the ResNet-50 (identity) features, images corresponding to the 10 largest classes of LFW are selected and t -distributed Stochastic Neighbor Embedding (t -SNE) is used to visualize the feature distributions (in 2D) before and after privacy enhancement. For the gender features 700 images from LFW are randomly sampled from the dataset for each gender.

The t -SNE plots in Fig. 9 show that both gender (top row) as well as subjects/identities (bottom row) are well separated with the original images. After privacy enhancement with k -AAP and FGSM most of the separation between subjects is preserved. The gender distributions, on the other hand, are less clustered and now exhibit a multimodal distribution. Nevertheless, the overlap between the male and female data points is still limited, indicating that the two classes can still be distinguished using a suitable classification model. These observations support the results from the previous section where only small values in IL scores were observed with these two techniques, while the ROC curves from the gender-recognition experiments showed good separation, but with inverted labels.

When looking at the FlowSAN models, a different be-

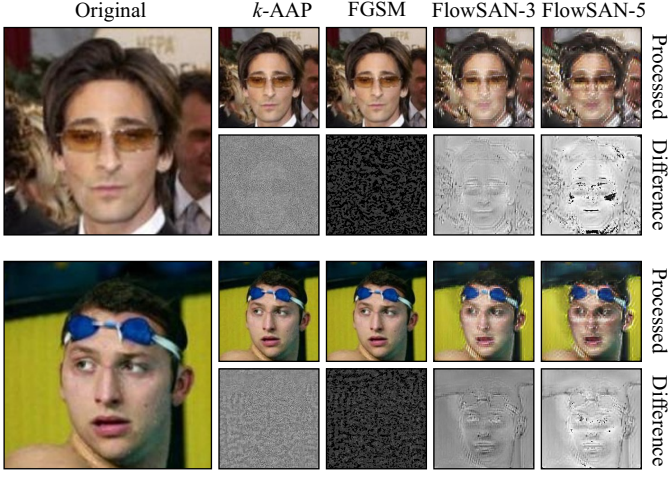


Fig. 10: Illustration of the visual effect of the privacy models on two sample images from LFW. The top row next to each original image shows the privacy-enhanced images (with gender privacy), whereas the bottom row depicts the difference between the original and the modified images. The difference was scaled for visualization purposes (by $10\times$ for k -AAP, $40\times$ for FGSM and $1\times$ for the FlowSAN models) and then normalized to the valid image range. Note that k -AAP and FGSM result in imperceptible appearance changes, while the FlowSAN models introduce visible changes.

havior can be observed. Here, the identity features are not well separated, but for many data points exhibit (reasonably) correct pair-wise similarities. The gender distributions, on the other hand, overlap significantly, with a higher overlap for the FlowSAN-5 model, which is expected given the objective of the privacy enhancement. The observed distributions explain the larger IL values for the FlowSAN models compared to k -AAP and FGSM in Figs. 8, but also point to the shortcoming of the adversarial techniques k -AAP and FGSM, where the (gender) label swap could easily be identified using manual inspection of a few sample images. This is not the case with the FlowSAN models.

4.3.3 Qualitative assessment

The impact of the privacy models on the visual appearance of a couple of sample images from the LFW dataset is shown in Fig. 10. As can be seen, k -AAP and FGSM generate privacy-enhanced images that appear almost identical to the original images, whereas the FlowSAN models introduce bigger and visually noticeable changes. The bottom row in each of the two examples presents a visualization of the changes introduced by the privacy models. k -AAP and FGSM add a relatively uniformly distributed noise pattern to the input images, while the FlowSAN models introduce a structured pattern focused predominantly on the facial area and less so on the background. This observation can be attributed to the design of the privacy models, where FlowSAN is designed specifically for facial images, while the other two models are applicable to arbitrary images and classification problems and, hence, are not designed to target specific visual categories, i.e., faces. From a qualitative perspective, the adversarial models have a clear edge over the FlowSAN model, but as suggested in the previous sec-

tions this edge comes at the expense of robustness to unseen classification models and the simpler privacy mechanism that aim to induce an incorrect prediction with a chosen classifier.

4.4 Robustness to Recovery Attempts

The main contribution of this study is a rigorous evaluation of existing (soft-biometric) privacy models with respect to their performance beyond zero-effort recognition experiments. The next series of experiments, therefore, explores the robustness of the evaluated models against attribute recovery attempts facilitated by our PrivacyProber.

4.4.1 One-Stage and Two-Stage Attribute Recovery

Multiple versions of PrivacyProber are implemented for the robustness experiments using either *one-stage* or *two-stage* attribute recovery. The simpler one-stage implementations consist of a single (generative or domain-specific) transformation, whereas the more complex two-stage implementations use sequential combinations of generative and domain-specific operations. For the one-stage implementations inpainting, super-resolution, denoising and background removal are considered as stand-alone recovery options, whereas multiple different combination of image transformations are incorporated into the two-stage implementations. A high-level overview of the studied PrivacyProber variants is presented in Table 3. Note that these combinations are not exhaustive with respect to all possible attribute recovery options discussed in Section 3. However, they do provide a representative cross-section of the existing options for the experimental evaluation.

For the implementation of the recovery techniques state-of-the-art backbone models are selected. Specifically, the GMCNN model⁶ [53] trained on CelebA-HQ [54] is utilized for the inpainting procedure, the C-SRIP⁷ [55] model trained on Casia WebFaces [56] is used for the super-resolution procedure, the WDnCNN⁸ [57] model trained on the Waterloo Exploration Database [58], the Berkeley segmentation dataset [59] and part of ImageNet [60] is chosen for the denoising operation and the DeepLabv3⁹ face parser [61] trained on CelebAMask-HQ [62] is selected for the background removal process. The backbone techniques ensure state-of-the-art performance for each task and come with publicly available implementations and pretrained weights. It is also important to note that the data used to train the backbone techniques does not overlap (in terms of images or subjects) with any of the test datasets used.

The impact of different PrivacyProbers on the visual appearance of a sample face images is presented in Fig. 11. Here, the numbers below the images correspond to probabilities that the subject on the image is male and the color coded frames indicate whether a gender classifier with a decision threshold at 0.5 correctly determines the subject's

6. GMCNN: https://github.com/shepnerd/inpainting_gmcnn

7. C-SRIP: <https://lmi.fe.uni-lj.si/en/research/fh/>

8. WDnCNN: <https://github.com/lixiaopeng123456/WDnCNN>

9. DeepLabv3: <https://github.com/tensorflow/models/tree/master/research/deeplab>

TABLE 3: PrivacyProber variants implemented for the experimental evaluation. The models differ in terms of whether generative or domain-specific components and whether one or two processing steps are utilized for attribute recovery.

PrivacyProber	χ	Generative components			Domain components	Characteristic
		Denoising	Inpainting	Super-resolution	Background removal	
PP-D	χ_d	✓	✗	✗	✗	Generative, one-stage (GOS)
PP-I	χ_{in}	✗	✓	✗	✗	Generative, one-stage (GOS)
PP-S	χ_{sr}	✗	✗	✓	✗	Generative, one-stage (GOS)
PP-B	χ_{br}	✗	✗	✗	✓	Domain-specific, one-stage (DOS)
PP-DI	$\chi_d \circ \chi_{in}$	✓	✓	✗	✗	Generative, two-stage (GTS)
PP-DS	$\chi_d \circ \chi_{sr}$	✓	✗	✓	✗	Generative, two-stage (GTS)
PP-DB	$\chi_d \circ \chi_{br}$	✓	✗	✗	✓	Generative+domain-specific, two-stage (GDT)
PP-IB	$\chi_{in} \circ \chi_{br}$	✗	✓	✗	✓	Generative+domain-specific, two-stage (GDT)
PP-SB	$\chi_{sr} \circ \chi_b$	✗	✗	✓	✓	Generative+domain-specific, two-stage (GDT)

◦ denotes a function composition operator.

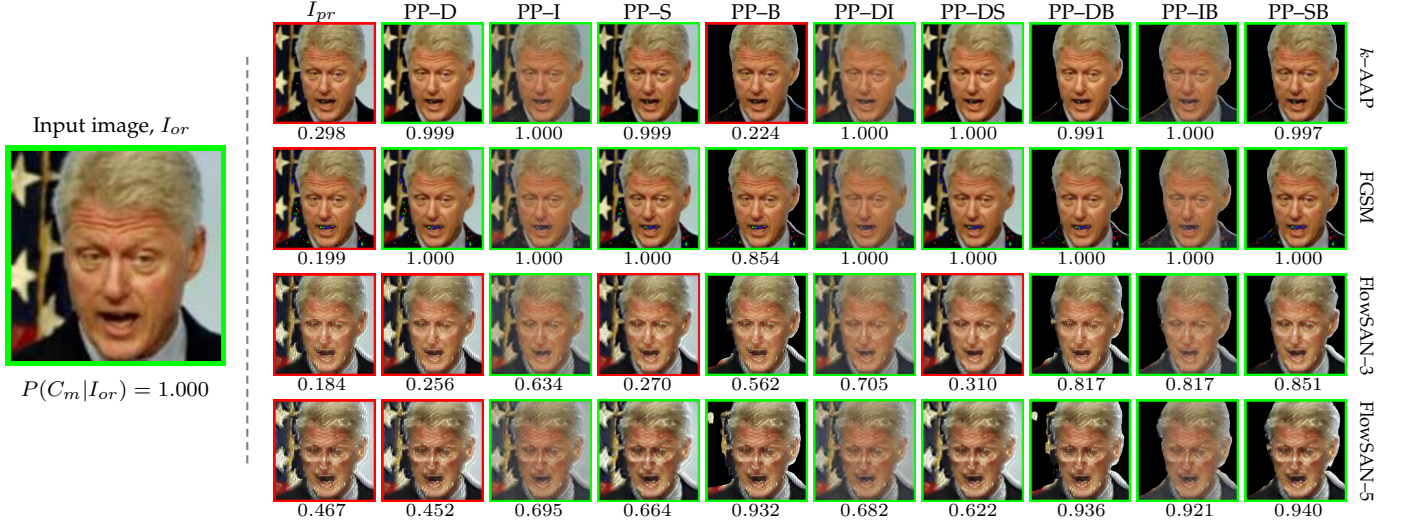


Fig. 11: Examples of PrivacyProber reconstructions, where the goal is to recover gender information from privacy-enhanced images. The number below each image corresponds to the probability output of a gender classifier – probabilities between 0–0.5 correspond to female and 0.5–1 to male subjects. Note that the privacy enhanced images, I_{pr} , generate incorrect gender probabilities (indicated by the red frames). PrivacyProber, on the other hand, recovers the correct gender information in most cases – indicated by the green frames. Depending on version of PrivacyProber images of different visual quality are generated.

gender (green) or not (red). As can be seen, most PrivacyProbers successfully recover gender information regardless of the privacy model used. The one-stage implementations based on inpainting (PP-I), super-resolution (PP-S) and denoising (PP-D) retain all of the visible semantic content. In terms of image quality, the inpainting scheme results in a slight loss of image contrast, whereas the denoising and especially super-resolution-based implementation additionally improve on the perceived quality of the facial images. Background subtraction is the only one-stage approach that removes part of the information and drastically changes the image content. Such images may be of limited use for certain applications, but can still facilitate automatic processing and analysis. The two-stage versions of PrivacyProber in general inherit the properties of the single-stage components and depending on the operations used may again retain all of the semantic content, e.g., PP-DS, PP-DI, or remove part of it due to background subtraction, e.g., PP-DB.

4.4.2 Robustness Analysis

To assess the robustness of the privacy models to attribute recovery attempts, privacy-enhanced images, I_{pr} , from all

three experimental datasets are first subjected to the implemented PrivacyProbers and then analyzed through verification and gender-recognition experiments. For the evaluation, the same gender classifier that steered the privacy enhancement on each dataset is again used to score gender-recognition performance. Note that the privacy models exhibited the strongest performance against this classifier (see Figs. 7 and 8), which makes attribute recovery particularly challenging. For the verification experiments, the ResNet-50 face recognition model is utilized.

1) ARR analysis. Table 4 presents the *attribute recovery robustness* (ARR) scores (from Eq. (11)) generated from the attribute-recovered images. For each privacy model (and for each dataset), ARR scores for the PrivacyProber that resulted in the lowest robustness are colored red and the scores that correspond to the highest robustness are colored blue. Several interesting observations can be made from the presented results: (i) First, considerably more information can be recovered from the adversarial techniques, k -AAP and FGSM, than from the FlowSAN models. For these techniques at least one of the PrivacyProbers results in a

TABLE 4: Attribute recovery robustness (ARR - higher scores indicate better robustness) scores generated for the evaluated privacy models with different PrivacyProber variants. Results are presented in terms of $(\mu \pm \sigma)$ ARR scores computed over 4 experimental splits and grouped by PrivacyProber type: GOS – Generative and One Stage; GDT – Generative and Two Stage; GDS – Generative and Domain-specific and Two Stage. The lowest robustness against attribute recovery for each privacy model on each dataset (in rows) is marked red, the highest is marked blue.

Privacy Model	Dataset	ARR – GOS models				ARR – GTS models		ARR – GDT models		
		PP-D	PP-I	PP-S	PP-B	PP-DI	PP-DS	PP-DB	PP-IB	PP-SB
<i>k</i> -AAP	LFW	0.157 \pm 0.086	0.070 \pm 0.042	0.343 \pm 0.111	0.402 \pm 0.099	0.045 \pm 0.024	0.081 \pm 0.063	0.069 \pm 0.059	0.051 \pm 0.004	0.166 \pm 0.096
	MUCT	0.048 \pm 0.030	0.045 \pm 0.025	0.342 \pm 0.085	0.908 \pm 0.016	0.093 \pm 0.012	0.059 \pm 0.035	0.053 \pm 0.039	0.060 \pm 0.026	0.182 \pm 0.082
	Adience	0.902 \pm 0.018	0.385 \pm 0.030	0.985 \pm 0.007	0.961 \pm 0.009	0.325 \pm 0.032	0.835 \pm 0.024	0.785 \pm 0.021	0.297 \pm 0.044	0.897 \pm 0.021
FGSM	LFW	0.032 \pm 0.025	0.080 \pm 0.020	0.271 \pm 0.057	0.599 \pm 0.032	0.103 \pm 0.014	0.066 \pm 0.024	0.066 \pm 0.020	0.089 \pm 0.018	0.046 \pm 0.039
	MUCT	0.110 \pm 0.018	0.113 \pm 0.008	0.099 \pm 0.059	0.817 \pm 0.040	0.125 \pm 0.003	0.117 \pm 0.011	0.113 \pm 0.015	0.117 \pm 0.006	0.038 \pm 0.027
	Adience	0.373 \pm 0.030	0.138 \pm 0.008	0.728 \pm 0.024	0.883 \pm 0.004	0.114 \pm 0.010	0.290 \pm 0.019	0.299 \pm 0.023	0.151 \pm 0.018	0.529 \pm 0.015
FlowSAN-3	LFW	0.237 \pm 0.031	0.228 \pm 0.021	0.194 \pm 0.041	0.234 \pm 0.042	0.247 \pm 0.032	0.204 \pm 0.050	0.251 \pm 0.038	0.371 \pm 0.027	0.241 \pm 0.039
	MUCT	0.183 \pm 0.095	0.109 \pm 0.130	0.066 \pm 0.091	0.058 \pm 0.053	0.124 \pm 0.129	0.091 \pm 0.115	0.103 \pm 0.090	0.082 \pm 0.081	0.065 \pm 0.029
	Adience	0.539 \pm 0.035	0.405 \pm 0.045	0.447 \pm 0.059	0.503 \pm 0.046	0.404 \pm 0.043	0.446 \pm 0.047	0.534 \pm 0.044	0.615 \pm 0.062	0.429 \pm 0.071
FlowSAN-5	LFW	0.549 \pm 0.062	0.400 \pm 0.053	0.441 \pm 0.052	0.508 \pm 0.072	0.414 \pm 0.046	0.447 \pm 0.052	0.511 \pm 0.064	0.493 \pm 0.047	0.451 \pm 0.071
	MUCT	0.642 \pm 0.063	0.567 \pm 0.123	0.541 \pm 0.042	0.559 \pm 0.071	0.536 \pm 0.116	0.557 \pm 0.060	0.485 \pm 0.069	0.479 \pm 0.150	0.457 \pm 0.045
	Adience	0.737 \pm 0.050	0.555 \pm 0.056	0.682 \pm 0.048	0.713 \pm 0.021	0.550 \pm 0.053	0.666 \pm 0.046	0.699 \pm 0.035	0.750 \pm 0.040	0.665 \pm 0.028

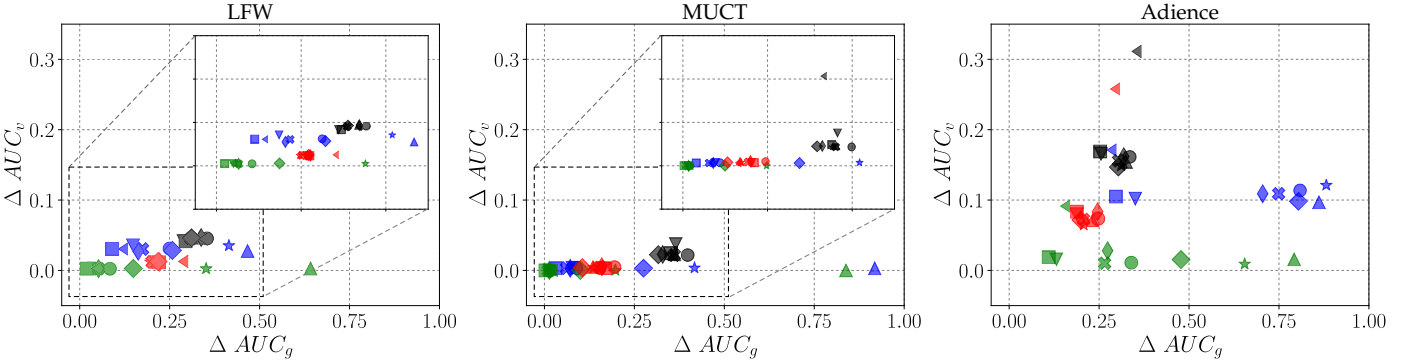


Fig. 12: Impact of application of different PrivacyProbers on the verification and gender-recognition performance. The x -axis shows the differences in verification performance observed with the original and privacy-enhanced images that were subjected to the proposed PrivacyProber, i.e., $\Delta AUC_v = AUC_{vo} - AUC_{vr}$. The y -axis shows a similar difference for gender recognition, i.e., $\Delta AUC_g = AUC_{go} - AUC_{gr}$. Results are presented across all tested privacy models, PrivacyProbers and experimental datasets. The figure is best viewed in color.

ARR score in the 0.1 range, which suggests that a significant amount of the gender information can be restored. Among the FlowSAN models, FlowSAN-3 is less robust to attribute recovery attempts than FlowSAN-5, but still significantly more so than *k*-AAP or FGSM. As expected, the most robust among all models is FlowSAN-5, where the weakest ARR scores across all PrivacyProbers are between 0.4 (on LFW) and 0.55 (on Adience). (ii) Second, the robustness of the privacy models varies from dataset to dataset. While the results on LFW and MUCT are relatively consistent, the weakest ARR scores on Adience are higher than the weakest scores on LFW and MUCT for all tested privacy models. This observation implies that attribute recovery robustness is in parts also affected by the initial data characteristics and not only by the recovery capabilities of the tested PrivacyProbers. Because the gender recognition performance was already weaker on Adience than on the remaining two datasets, even small degradations from the initial images, I_{or} , cause further degradations. This fact is then also reflected in the success of the attribute recovery attempts. (iii) Third, all evaluated PrivacyProbers are able to recover some level

of gender information from the privacy-enhanced images, suggesting that the reported performance with zero-effort evaluation scenarios typically reported in the literature often overestimates the actual capabilities of the existing privacy models. However, the most informative PrivacyProbers are the ones based on inpainting (PP-I), and combinations of denoising and inpainting (PP-DI), and super-resolution and background subtraction (PP-SB). These models are able to recover the most gender information (resulting in the lowest ARR scores overall – see scores colored red) and are, therefore, most informative when evaluating robustness of existing privacy models.

2) Attribute recovery vs. verification performance. The implemented PrivacyProbers aim to reconstruct attribute information and as a result alter the characteristics of the facial images. To analyze the impact of attribute recovery on the trade-off between identity preservation and attribute recovery robustness, we plot the difference in AUC scores between the original and the attribute-recovered images for both verification and gender recognition experiments in Fig. 12. Points indicating that all of the identity and

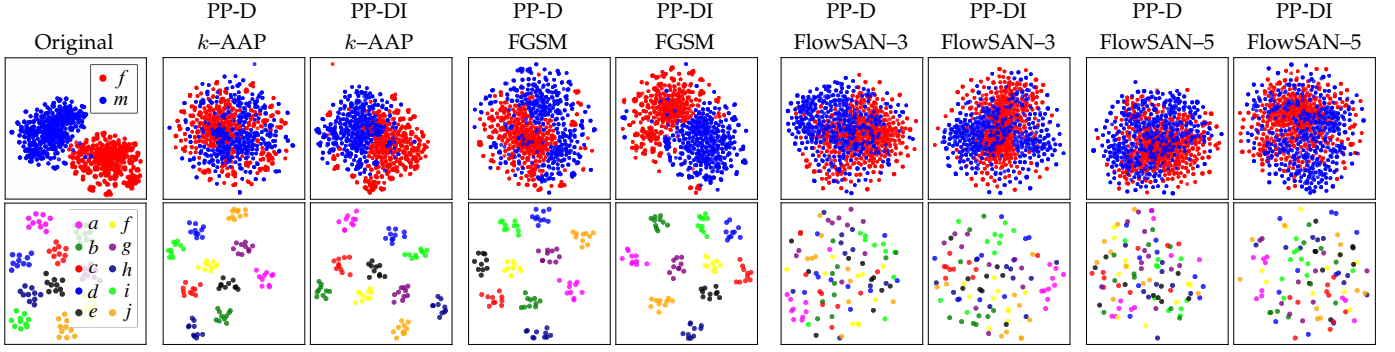


Fig. 13: t -SNE plots (in 2D) for gender and identity features. Results are presented for the original face images (far left) and images processed from with the best performing one-stage and two stage PrivacyProbers, i.e., PP-D and PP-DI. The gender in the top row are generated from 700 randomly sampled LFW images of each gender and the subject plots in the bottom row are generated based on 10 randomly selected images of the 10 largest LFW classes. Best viewed in color.

gender information contained in the original images was recovered are located at the origin of the plots. These points correspond to the least robust privacy models. Different from the scalar ARR scores analyzed in the previous section, the presented plots offer more insight into the behavior of the tested models, but also the characteristics of the attribute recovery attempts.

As can be seen from Fig. 12, the information content can be restored to close to the same level as before the privacy enhancement with k -AAP and FGSM on LFW and MUCT given the most effective PrivacyProbers. On these two datasets, FlowSAN-3-recovered images perform similarly to the original ones in terms of verification performance, but still offer a certain level of soft-biometric privacy. This result points to the robustness of the privacy model, but also shows that gender information can be recovered without affecting identity cues. FlowSAN-5 exhibits the greatest level of robustness to recovery attempts, but at the expense of the largest loss of identity information among all models. On Adience, similar observations can be made for FGSM, which is again the least robust of all tested privacy models. k -AAP, FlowSAN-3 and FlowSAN-5 exhibit higher levels of robustness, i.e., ΔAUC_g is comparably larger, but these appear to be a consequence of a general loss of useful visual information, as indicated by the drop in the verification performance compared to the original images. Among the PrivacyProbers, the most effective (on average) for the robustness analysis, with respect to both gender and identity information, is again PP-DI. The combination of image denoising and context-based inpainting appears to be highly effective in reconstructing attribute information and for evaluating the robustness of soft-biometric privacy models, though other types of attribute recovery may offer additional insights.

4.4.3 Attribute Recovery and Feature Distributions

Attribute recovery attempts change the visual characteristics of facial images, as illustrated in Fig. 10. Because these changes also affect the feature representations generated by the recognition models, we next analyze the feature distributions generated from the attribute-recovered images. Fig. 13 compares the t -SNE based distributions produced by the face and gender-recognition models. Here, the same setup (involving LFW) as in Section 4.3.2 is utilized to

generate feature vectors for the plots. To keep the analysis concise only the best performing one- and two-stage PrivacyProbers are considered, i.e., PP-D and PP-DI.

The presented plots support the observation made in the previous section. Attribute recovery (with PP-D and PP-DI) contributes towards well separated gender classes in the feature space for k -AAP and FGSM with minimal impact of the separability of the identity classes. For FlowSAN-3 and FlowSAN-5 we see less gender separation due to higher robustness of the privacy models and again minimal impact on identity information.

4.5 Detecting (Soft-Biometric) Privacy Enhancement

In this section we now show that detecting privacy enhancement can be done efficiently using a simple scheme build around the proposed PrivacyProber. The detection scheme, illustrated in Fig. 14, exploits the fact that for privacy-enhanced images, I_{pr} , a selected gender (or attribute) classifier ξ generates different posterior probabilities $p(C_k|I_{pr})$ than for images processed with our PrivacyProber $p(C_k|I_{re})$, where $C_k \in \{C_m, C_f\}$ and m denotes the male and f the female class. By comparing the posteriors it is possible to determine whether an image has been tampered with or not. For the experiments presented below, the comparison is done based on a symmetric version of the Kullback-Leibler divergence [63], [64]:

$$D_{SKL}(p, q) = D_{KL}(p||q) + D_{KL}(q||p), \quad (13)$$

where

$$D_{KL}(p||q) = \sum_{x \in \mathcal{X}} p(x) \log \left(\frac{p(x)}{q(x)} \right) \quad (14)$$

where $p = p(C_k|I_{pr})$, $q = p(C_k|I_{re})$, $\mathcal{X} = C_k$ and D_{SKL} is used as a measure of tampering (or privacy enhancement).

Note that different from most existing schemes to image tampering detection, the proposed approach to Privacy-enhancement Detection with Prediction Divergence (PD²) is *training-free* and does not require any examples of tampered images. It relies solely on the observation that after attribute recovery, the output of a (in this case gender) classifier changes compared to the output produced with the initial face image. Thus, the detection scheme is expected to work, as long as the PrivacyProber causes a change in the (concealed) attribute information.

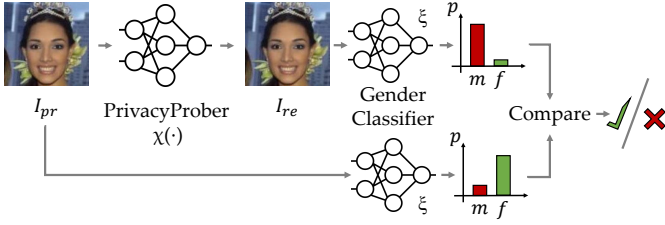


Fig. 14: Detection of privacy enhancements with the proposed PrivacyProber. The proposed PD² detection scheme exploits discrepancies between the classification predictions generated from the original and processed images. Unlike existing approaches to tampering detection, our scheme is learning-free and requires only prediction comparisons.

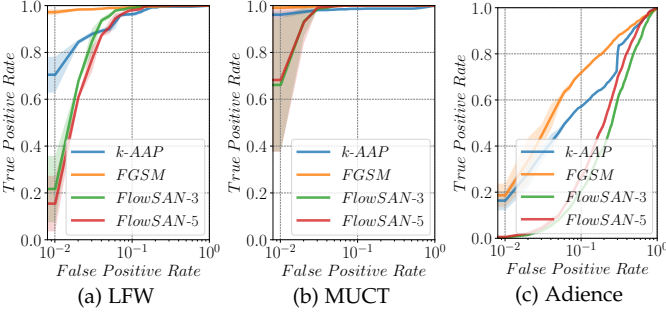


Fig. 15: ROC of privacy-enhancement detection experiments with PD² on LFW, MUCT and Adience. Note that k -AAP and FGSM based enhancements are detected more efficiently than the alterations from the FlowSAN models.

To evaluate the detection performance of PD², we select 698 privacy-enhanced and 698 original images for each of the considered privacy models and each dataset. The images are again partitioned into 4 disjoint experimental splits over which results are reported. PD² is implemented with the best performing PrivacyProber from the previous experiments, i.e., PP-DI, to keep the results uncluttered.

4.5.1 PD² Detection Performance

Fig. 15 plots the average ROC curves and corresponding confidence intervals over the four experimental splits for all privacy models and three datasets. To be able to visualize performance differences, the curves are presented on a semilog scale. The results show that PD² achieves close to ideal detection performance for all privacy models on LFW and MUCT and with average AUC scores of 0.828 for k -AAP, 0.877 for FGSM, 0.696 for FlowSAN-3 and 0.751 for FlowSAN-5 also does very well on Adience. The somewhat weaker results on Adience are a consequence of the challenging imaging characteristics that were already shown to affect all tasks evaluated earlier in the paper. Additionally, all privacy models exhibited the highest level of robustness on the Adience dataset, contributing to the difficulty of detecting tampering with PD².

4.5.2 Comparison with competing models

We note again that the problem of detecting privacy enhancement in facial images has, to the best of our knowledge, not yet been studied in the open literature. However,

because soft-biometric privacy enhancement techniques share some characteristics with adversarial attacks, we select the recent state-of-the-art transformation-based detection technique (denoted T-SVM hereafter) from [42] as a baseline for our experiments and compare it to PD². T-SVM combines features from the discrete wavelet (DWT) and discrete sine (DST) transforms with a support vector classifier (SVM) for tampering detection and requires training data to be able to learn how to discriminate between original and tampered images. We, therefore, consider several scenarios in the comparison, i.e.:

- **White-box evaluation:** With this strategy access to all privacy models is assumed. For the experiments, T-SVM is trained separately for each privacy model. The training part of LFW is used to learn the detection models, which is then tested on the test images of LFW as well as the MUCT and Adience datasets.
- **Black-box evaluation:** For this strategy access to some tampered images is assumed, but not to images of all privacy models. T-SVM, therefore, needs to generalize to unseen privacy models. Two distinct detection models are considered in the experiments. The first, T-SVM (A), is trained for detection of FlowSAN-5 enhanced image only on data from LFW. The second, T-SVM (B), is trained for detecting k -AAP based enhancement, again only on LFW. Both models are tested on all datasets and with all privacy models.

1) Quantitative comparison. Table 5 shows that in the white-box scenario T-SVM is comparable to PD² on LFW in terms of tampering detection for k -AAP and FGSM, but considerably worse on MUCT and Adience. This result suggests that despite access to examples of tampered images for each privacy model, the detection performance of T-SVM is significantly affected by the data characteristics, which is seen to a much lesser extent by the learning-free PD² approach. For the FlowSAN experiments, T-SVM offers perfect detection performance on all three datasets, PD² is close on LFW and MUCT, but falls behind on Adience. The presented results show that the generalization ability of the white box T-SVM detection technique is below PD² despite the access to tampered training examples for each privacy model, which are not needed by PD².

When looking at the AUC scores for the black-box experiments, we see that the detection results for T-SVM are in general weaker. T-SVM (A), which is trained with FlowSAN-5 tampered images, is still able to ensure ideal detection performance for both FlowSAN models on all datasets, but is less competitive for the detection of k -AAP and FGSM tampered images. For these privacy models the detection performance of T-SVM (A) drops slightly behind the white-box T-SVM and considerably behind PD². The T-SVM (B) models, trained with k -AAP images from LFW, is the least competitive and only able to match the performance of PD² for a few selected cases involving LFW. The presented results clearly show the added value of training-free tampering detection, where the detection performance is not affected by the available training data, which otherwise considerably affects the generalization capabilities of the detection techniques.

2) Visual analysis. Fig. 16 presents a few examples of

TABLE 5: AUC scores ($\mu \pm \sigma$) for privacy-enhancement detection experiments. The learning-free (black box) PD² approach is compared against the classification-based T-SVM techniques for adversarial attack detection from [42]. Both white-box and black-box comparisons are presented.

Privacy Model	Dataset	PD ² (ours)	White box	Black box	
			T-SVM	T-SVM (A) [†]	T-SVM (B) [‡]
k -AAP	LFW	0.980 \pm 0.003	0.984 \pm 0.007	0.743 \pm 0.013	0.984 \pm 0.007
	MUCT	0.984 \pm 0.001	0.534 \pm 0.021	0.727 \pm 0.030	0.534 \pm 0.021
	Adience	0.828 \pm 0.002	0.541 \pm 0.007	0.604 \pm 0.008	0.541 \pm 0.007
FGSM	LFW	0.992 \pm 0.001	0.955 \pm 0.011	0.894 \pm 0.013	0.921 \pm 0.016
	MUCT	0.995 \pm 0.000	0.852 \pm 0.012	0.858 \pm 0.015	0.552 \pm 0.030
	Adience	0.877 \pm 0.004	0.624 \pm 0.009	0.595 \pm 0.016	0.471 \pm 0.014
FlowSAN-3	LFW	0.980 \pm 0.002	1.000 \pm 0.000	1.000 \pm 0.000	0.997 \pm 0.002
	MUCT	0.991 \pm 0.003	1.000 \pm 0.000	1.000 \pm 0.000	0.524 \pm 0.020
	Adience	0.696 \pm 0.003	1.000 \pm 0.000	1.000 \pm 0.000	0.609 \pm 0.005
FlowSAN-5	LFW	0.976 \pm 0.002	1.000 \pm 0.000	1.000 \pm 0.000	0.998 \pm 0.001
	MUCT	0.991 \pm 0.004	1.000 \pm 0.000	1.000 \pm 0.000	0.531 \pm 0.018
	Adience	0.751 \pm 0.003	1.000 \pm 0.000	1.000 \pm 0.000	0.563 \pm 0.005

[†] Detection model trained on FlowSAN-5 and LFW.

[‡] Detection model trained on k -AAP and LFW.

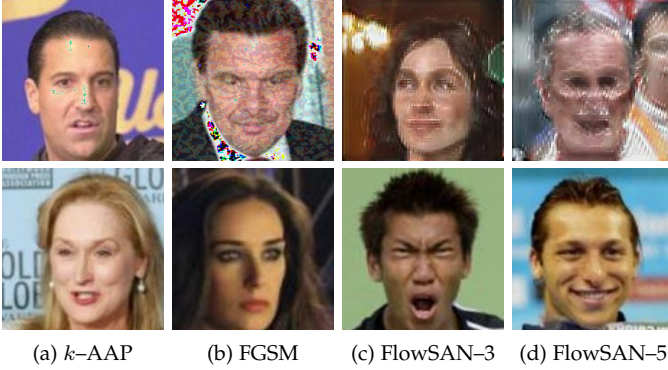


Fig. 16: Examples of misdetections by PD². The top row shows images where PD² did not detect the privacy enhancement and the bottom row shows examples where PD² incorrectly flagged non-tampered images.

face images, where the PD² approach did not correctly detect the presence of image tampering (i.e., privacy enhancement) at a decision threshold that ensures equal error rates with the ROC curves from Fig. 15. Here, the top row shows example images where PD² failed to detect privacy enhanced images. In most cases, these images contain visible image artifacts that cannot be recovered using the restoration approaches in PP-DI, resulting in minimal changes in the gender prediction and consequently misdetections. The bottom row shows example images that have been flagged by PD² as being tampered, but in fact represent original images. As can be seen, such images are of poor quality (due to blur, noise, etc.) and get improved by PP-DI. As a result, the output of the gender classifier changes enough to flag the images as tampered. While the performance of PD² is highly competitive (and close to ideal on most datasets), the presented examples suggest that there is room for further improvement by, for example, combining PD² with supervised detection techniques that should be able to perform well with poor quality images. Such a combination is explored in the Supplementary material of the paper.

5 CONCLUSION

In this study we investigated the reliability of state-of-the-art soft-biometric privacy-enhancing techniques and explored their robustness to attribute recovery attempts. We introduced PrivacyProber, a framework for the recovery of suppressed soft-biometric information from facial images, and used it in a comprehensive experimental evaluation. Experimental results on the LFW, MUCT and Adience datasets showed that there are considerable differences between the tested privacy models, both in terms of visual impact on the privacy-enhanced images as well as in terms of the level of privacy ensured. Additionally, we observed that (using our framework) it was possible to recover a considerable amount of suppressed (concealed) attribute information regardless of the privacy model used. However, the robustness of the tested synthesis-based techniques (i.e., FlowSANs) was observed to be considerable higher than that of the evaluated adversarial approaches (i.e., k -AAP and FGSM). These findings have considerable implications for future research in the area of biometric privacy enhancement, where more work is needed to improve robustness of existing models.

As another contribution, we showed that the proposed attribute recovery framework can also be used to detect privacy enhancement (e.g., tampering) in facial images. We proposed, to the best of our knowledge, the first approach for this task, i.e., PD², and demonstrated that it can detect privacy enhancements with high accuracy even if different privacy models are utilized and data with diverse characteristics is used. This fact points to another threat vector with respect to biometric privacy models in that privacy-enhanced images can easily be identified and subjected to alternative means of processing that is less sensitive to artifacts and perturbations infused with the enhancement.

As part of our future work, we plan to extend our robustness analysis to other biometric privacy models, e.g., deidentification techniques, which are based on different assumptions and require conceptually different models to restore the obscured information.

ACKNOWLEDGMENTS

This research was supported in parts by the ARRS Project J2-1734 “Face deidentification with generative deep models”, ARRS Research Programs P2-0250 (B) “Metrology and Biometric Systems” and P2-0214 (A) “Computer Vision”.

REFERENCES

- [1] A. Dantcheva, P. Elia, and A. Ross, “What Else Does Your Biometric Data Reveal? A Survey on Soft Biometrics,” *IEEE Transactions on Information Forensics and Security (TIFS)*, vol. 11, no. 3, pp. 441–467, 2015.
- [2] R. Ranjan, V. M. Patel, and R. Chellappa, “Hyperfacer: A Deep Multi-task Learning Framework for Face Detection, Landmark Localization, Pose Estimation, and Gender Recognition,” *IEEE Transactions on Pattern Analysis and Machine Intelligence (TPAMI)*, vol. 41, no. 1, pp. 121–135, 2017.
- [3] H. Pan, H. Han, S. Shan, and X. Chen, “Mean-variance Loss for Deep Age Estimation from a Face,” in *IEEE Conference on Computer Vision and Pattern Recognition (CVPR)*, 2018, pp. 5285–5294.
- [4] Z. Niu, M. Zhou, L. Wang, X. Gao, and G. Hua, “Ordinal Regression with Multiple Output CNN for Age Estimation,” in *IEEE Conference on Computer Vision and Pattern Recognition (CVPR)*, 2016, pp. 4920–4928.
- [5] F. H. d. B. Zavan, O. R. Bellon, L. Silva, and G. G. Medioni, “Benchmarking Parts Based Face Processing In-The-Wild for Gender Recognition and Head Pose Estimation,” *Pattern Recognition Letters*, vol. 123, pp. 104–110, 2019.
- [6] N. Berthouze, M. Valstar, A. Williams, J. Egede, T. Olugbade, C. Wang, H. Meng, M. Aung, N. Lane, and S. Song, “Emopain Challenge 2020: Multimodal Pain Evaluation from Facial and Bodily Expressions,” in *IEEE Conference on Automatic Face and Gesture Recognition (FG)*, 2020.
- [7] P. Li, P. J. Flynn, L. Prieto, and D. Mery, “Face Recognition in Low Quality Images: A Survey,” *ACM Computing Surveys*, vol. 1, no. 1, 2019.
- [8] L. Mao, Y. Yan, J.-H. Xue, and H. Wang, “Deep Multi-task Multi-label CNN for Effective Facial Attribute Classification,” *IEEE Transactions on Affective Computing (TAC)*, 2020.
- [9] A. Jobin, M. Ienca, and E. Vayena, “The Global Landscape of AI Ethics Guidelines,” *Nature Machine Intelligence*, vol. 1, no. 9, pp. 389–399, 2019.
- [10] R. Singh, M. Vatsa, and N. Ratha, “Trustworthy AI,” in *8th ACM IKDD CODS and 26th COMAD*, 2021, pp. 449–453.
- [11] V. Mirjalili, S. Raschka, and A. Ross, “FlowSAN: Privacy-enhancing Semi-adversarial Networks to Confound Arbitrary Face-based Gender Classifiers,” *IEEE Access*, vol. 7, pp. 99 735–99 745, 2019.
- [12] S. Chhabra, R. Singh, M. Vatsa, and G. Gupta, “Anonymizing k-Facial Attributes via Adversarial Perturbations,” *International Joint Conferences on Artificial Intelligence (IJCAI)*, 2018.
- [13] B. Meden, P. Rot, P. Terhörst, N. Damer, A. Kuijper, W. Scheirer, A. Ross, P. Peer, and V. Štruc, “Privacy-Enhancing Face Biometrics: A Comprehensive Survey,” *under review*, 2021.
- [14] V. Mirjalili, S. Raschka, and A. Ross, “PrivacyNet: Semi-adversarial Networks for Multi-attribute Face Privacy,” *IEEE Transactions on Image Processing (TIP)*, vol. 29, pp. 9400–9412, 2020.
- [15] P. Terhörst, K. Riehl, N. Damer, P. Rot, B. Bortolato, F. Kirchbuchner, V. Štruc, and A. Kuijper, “PE-MIU: A Training-free Privacy-enhancing Face Recognition Approach Based on Minimum Information Units,” *IEEE Access*, 2020.
- [16] B. Bortolato, M. Ivanovska, P. Rot, J. Krizaj, P. Terhörst, N. Damer, P. Peer, and V. Štruc, “Learning Privacy-enhancing Face Representations Through Feature Disentanglement,” in *IEEE International Conference on Automatic Face and Gesture Recognition (FG)*, 2020.
- [17] P. Voigt and A. v. d. Bussche, *The EU General Data Protection Regulation (GDPR): A Practical Guide*, 1st ed. Springer, 2017.
- [18] P. Bukaty, *The California Consumer Privacy Act (CCPA): An implementation guide*. IT Governance Publishing, 2019.
- [19] 740 ILCS/14, “Biometric Information Privacy Act (BIPA),” Illinois General Assembly, Public Act 095-994, 2008.
- [20] A. Othman and A. Ross, “Privacy of Facial Soft Biometrics: Suppressing Gender but Retaining Identity,” in *European Conference on Computer Vision (ECCV)*. Springer, 2014, pp. 682–696.
- [21] V. Mirjalili, S. Raschka, A. Namboodiri, and A. Ross, “Semi-Adversarial Networks: Convolutional Autoencoders for Imparting Privacy to Face Images,” in *International Conference on Biometrics (ICB)*, 2018, pp. 82–89.
- [22] A. Rozsa, M. Günther, E. M. Rudd, and T. E. Boulton, “Facial Attributes: Accuracy and Adversarial Robustness,” *Pattern Recognition Letters*, vol. 124, pp. 100–108, 2019.
- [23] T. Winkler and B. Rinner, “Security and Privacy Protection in Visual Sensor Networks: A Survey,” *ACM Computing Surveys*, vol. 47, no. 1, 2014.
- [24] J. R. Padilla-López, A. A. Chaaoui, and F. Flórez-Revuelta, “Visual Privacy Protection Methods: A Survey,” *Expert Systems with Applications*, vol. 42, no. 9, pp. 4177 – 4195, 2015.
- [25] S. L. Garfinkel, “De-identification of Personal Information,” *National Institute of Standards and Technology (NIST)*, 2015.
- [26] S. Ribarić, A. Ariyaeinia, and N. Pavesić, “De-identification for Privacy Protection in Multimedia Content: A Survey,” *Signal Processing: Image Communication*, vol. 47, pp. 131 – 151, 2016.
- [27] P. Terhörst, N. Damer, F. Kirchbuchner, and A. Kuijper, “Un-supervised Privacy-enhancement of Face Representations using Similarity-sensitive Noise Transformations,” *Applied Intelligence*, pp. 1–18, 2019.
- [28] P. Terhörst, M. Huber, N. Damer, P. Rot, F. Kirchbuchner, V. Štruc, and A. Kuijper, “Privacy Evaluation Protocols for the Evaluation of Soft-Biometric Privacy-Enhancing Technologies,” *International Conference of the Biometrics Special Interest Group (BIOSIG)*, 2020.
- [29] A. Morales, J. Fierrez, R. Vera-Rodriguez, and R. Tolosana, “SensitiveNets: Learning Agnostic Representations with Application to Face Images,” *IEEE Transactions on Pattern Analysis and Machine Intelligence (TPAMI)*, 2020.
- [30] P. Terhörst, N. Damer, F. Kirchbuchner, and A. Kuijper, “Suppressing Gender and Age in Face Templates Using Incremental Variable Elimination,” in *International Conference on Biometrics (ICB)*, 2019, pp. 4–7.
- [31] V. Mirjalili and A. Ross, “Soft Biometric Privacy: Retaining Biometric Utility of Face Images While Perturbing Gender,” in *International Joint Conference on Biometrics (IJCB)*, 2017, pp. 564–573.
- [32] N. Carlini and D. Wagner, “Towards Evaluating the Robustness of Neural Networks,” in *IEEE Symposium on Security and Privacy (SP)*, 2017, pp. 39–57.
- [33] I. Goodfellow, J. Shlens, and C. Szegedy, “Explaining and Harnessing Adversarial Examples,” in *International Conference on Learning Representations*, 2015.
- [34] P. Dhar, A. Bansal, C. D. Castillo, J. Gleason, P. J. Phillips, and R. Chellappa, “How Are Attributes Expressed in Face DCNNs?” in *IEEE International Conference on Automatic Face and Gesture Recognition (FG)*, 2020, pp. 85–92.
- [35] L. Zheng, Y. Zhang, and V. L. Thing, “A Survey on Image Tampering and its Detection in Real-world Photos,” *Journal of Visual Communication and Image Representation*, vol. 58, pp. 380–399, 2019.
- [36] K. A. da Costa, J. P. Papa, L. A. Passos, D. Colombo, J. Del Ser, K. Muhammad, and V. H. C. de Albuquerque, “A Critical Literature Survey and Prospects on Tampering and Anomaly Detection in Image Data,” *Applied Soft Computing*, 2020.
- [37] K. B. Meena and V. Tyagi, “Image Forgery Detection: Survey and Future Directions,” in *Data, Engineering and applications*. Springer, 2019, pp. 163–194.
- [38] E. Nowroozi, A. Dehghantanha, R. M. Parizi, and K.-K. R. Choo, “A Survey of Machine Learning Techniques in Adversarial Image Forensics,” *Computers and Security*, 2020.
- [39] S. Bulusu, B. Kailkhura, B. Li, P. Varshney, and D. Song, “Anomalous Example Detection in Deep Learning: A Survey,” *IEEE Access*, vol. 8, pp. 132 330–132 347, 2020.
- [40] X. Wang, J. Li, X. Kuang, Y.-a. Tan, and J. Li, “The Security of Machine Learning in an Adversarial Setting: A Survey,” *Journal of Parallel and Distributed Computing*, vol. 130, pp. 12–23, 2019.
- [41] A. Chakraborty, M. Alam, V. Dey, A. Chattopadhyay, and D. Mukhopadhyay, “Adversarial Attacks and Defences: A Survey,” *CoRR*, vol. abs/1810.00069, 2018.
- [42] A. Agarwal, R. Singh, M. Vatsa, and N. K. Ratha, “Image Transformation Based Defense Against Adversarial Perturbation on Deep Learning Models,” *IEEE Transactions on Dependable and Secure Computing (TDSC)*, 2020.
- [43] A. Mustafa, S. H. Khan, M. Hayat, J. Shen, and L. Shao, “Image Super-Resolution as a Defense Against Adversarial Attacks,” *IEEE Transactions on Image Processing (TIP)*, vol. 29, pp. 1711–1724, 2019.

- [44] P. Gupta and E. Rahtu, "CIIDefence: Defeating Adversarial Attacks by Fusing Class-Specific Image Inpainting and Image Denoising," in *IEEE International Conference on Computer Vision (ICCV)*, 2019.
- [45] S. Baker and T. Kanade, "Hallucinating Faces," in *IEEE International Conference on Automatic Face and Gesture Recognition (FG)*, 2000, pp. 83–88.
- [46] K. Grm, M. Pernuš, L. Cluzel, W. J. Scheirer, S. Dobrišek, and V. Štruc, "Face Hallucination Revisited: An Exploratory Study on Dataset Bias," in *IEEE Conference on Computer Vision and Pattern Recognition Workshops (CVPR)*, 2019.
- [47] E. Chatzikiriakidis, C. Papaioannidis, and I. Pitas, "Adversarial Face De-Identification," in *IEEE International Conference on Image Processing (ICIP)*, 2019, pp. 684–688.
- [48] G. B. Huang, M. Ramesh, T. Berg, and E. Learned-Miller, "Labeled Faces in the Wild: A Database for Studying Face Recognition in Unconstrained Environments," University of Massachusetts, Amherst, Tech. Rep. 07-49, 2007.
- [49] S. Milborrow, J. Morkel, and F. Nicolls, "The MUCT Landmarked Face Database," *Pattern Recognition Association of South Africa*, 2010, <http://www.milbo.org/muct>.
- [50] E. Eidinger, R. Enbar, and T. Hassner, "Age and Gender Estimation of Unfiltered Faces," *IEEE Transactions on Information Forensics and Security (TIFS)*, vol. 9, no. 12, pp. 2170–2179, 2014.
- [51] V. Mirjalili, S. Raschka, and A. Ross, "Gender Privacy: An Ensemble of Semi Adversarial Networks for Confounding Arbitrary Gender Classifiers," *IEEE International Conference on Biometrics Theory, Applications and Systems (BTAS)*, pp. 1–10, 2018.
- [52] Q. Cao, L. Shen, W. Xie, O. M. Parkhi, and A. Zisserman, "VG-FA2: A Dataset for Recognising Faces Across Pose and Age," in *IEEE International Conference on Automatic Face and Gesture Recognition (FG)*, 2018, pp. 67–74.
- [53] Y. Wang, X. Tao, X. Qi, X. Shen, and J. Jia, "Image Inpainting via Generative Multi-column Convolutional Neural Networks," in *Advances in Neural Information Processing Systems (NIPS)*, 2018, pp. 331–340.
- [54] T. Karras, T. Aila, S. Laine, and J. Lehtinen, "Progressive Growing of GANs for Improved Quality, Stability, and Variation," *CoRR*, vol. abs/1710.10196, 2017.
- [55] K. Grm, W. J. Scheirer, and V. Štruc, "Face Hallucination Using Cascaded Super-Resolution and Identity Priors," *IEEE Transactions on Image Processing (TIP)*, vol. 29, pp. 2150–2165, 2020.
- [56] D. Yi, Z. Lei, S. Liao, and S. Z. Li, "Learning Face Representation from Scratch," *CoRR*, vol. abs/1411.7923, 2014.
- [57] R. Zhao, K. Lam, and D. P. K. Lun, "Enhancement of a CNN-Based Denoiser Based on Spatial and Spectral Analysis," in *IEEE International Conference on Image Processing (ICIP)*, Sep. 2019, pp. 1124–1128.
- [58] K. Ma, Z. Duanmu, Q. Wu, Z. Wang, H. Yong, H. Li, and L. Zhang, "Waterloo Exploration Database: New Challenges for Image Quality Assessment Models," *IEEE Transactions on Image Processing (TIP)*, vol. 26, no. 2, pp. 1004–1016, 2017.
- [59] S. Roth and M. J. Black, "Fields of Experts: A Framework for Learning Image Priors," in *IEEE Computer Society Conference on Computer Vision and Pattern Recognition (CVPR)*, vol. 2, 2005, pp. 860–867 vol. 2.
- [60] J. Deng, W. Dong, R. Socher, L. Li, Kai Li, and Li Fei-Fei, "ImageNet: A Large-scale Hierarchical Image Database," in *IEEE Conference on Computer Vision and Pattern Recognition (CVPR)*, 2009, pp. 248–255.
- [61] L. Chen, G. Papandreou, F. Schroff, and H. Adam, "Rethinking Atrous Convolution for Semantic Image Segmentation," *CoRR*, vol. abs/1706.05587, 2017.
- [62] C.-H. Lee, Z. Liu, L. Wu, and P. Luo, "MaskGAN: Towards Diverse and Interactive Facial Image Manipulation," in *IEEE Conference on Computer Vision and Pattern Recognition (CVPR)*, 2020.
- [63] D. Johnson and S. Sinanovic, "Symmetrizing the Kullback-leibler Distance," *IEEE Transactions on Information Theory (IT)*, 2001.
- [64] B. Bigi, "Using Kullback-Leibler Distance for Text Categorization," in *European Conference on Information Retrieval (ECIR)*, 2003.



Peter Rot is a researcher at the Laboratory for Machine Intelligence, Faculty of Electrical Engineering, and the Laboratory for Computer Vision, Faculty of Computer and Information Science, University of Ljubljana, Slovenia. He received his Bachelor's (2015) and Master's (2018) degrees from the Faculty of Computer and Information Science and he is currently pursuing a PhD in computer science at the University of Ljubljana. During his undergraduate studies he completed several internships, including internships at the Jozef Stefan Institute (Ljubljana, Slovenia) and Philips (Belfast, UK). His research interests include privacy aspects of face biometrics, sclera recognition and deep learning. Peter is a student member of the IEEE and a reviewer for top-tier conferences and journals, e.g., TIFS, FG and CVWW.



Peter Peer is a Professor of computer science at the University of Ljubljana, Slovenia, where he heads the Computer Vision Laboratory, coordinates the double degree study program with the Kyungpook National University, South Korea, and serves as a vice-dean for economic affairs. He received his doctoral degree in computer science from the University of Ljubljana in 2003. Within his post-doctorate he was an invited researcher at CEIT, Donostia – San Sebastian, Spain. His research interests include biometrics, color constancy, image segmentation, detection, recognition and real-time computer vision applications. He participated in several national and EU funded R&D projects and published more than 100 research papers in leading international peer reviewed journals and conferences. He is co-organizer of the Unconstrained Ear Recognition Challenge and Sclera Segmentation Benchmarking Competition. He serves as an Associated Editor of IEEE Access and IET Biometrics. He is a member of the EAB, IAPR and IEEE, where he also served as a chairman of the Slovenian IEEE Computer chapter for four years.



Vitomir Štruc is an Associate Professor at the University of Ljubljana, Slovenia. He received his doctoral degree from the Faculty of Electrical Engineering in Ljubljana in 2010. Vitomir's research interests include problems related to biometrics, computer vision, image processing, pattern recognition and machine learning. He (co-)authored more than 100 research papers for leading international peer reviewed journals and conferences in these and related areas. He served in different capacities on the organizing committees of several top-tier vision conferences, including IEEE Face and Gesture, ICB, WACV and IJCB. Vitomir is a Senior Area Editor for the IEEE Transactions on Information Forensics and Security, and an Associate Editor for Pattern Recognition, Signal Processing, and IET Biometrics. He served as an Area Chair for WACV 2018, 2019, 2020, ICPR 2018, Eusipco 2019 and FG 2020. Dr. Štruc is a member of the IEEE, IAPR, EURASIP, Slovenia's national contact point for the EAB and the current president of the Slovenian Pattern Recognition Society (Slovenian branch of IAPR).